DEVELOPING HYDROGELS WITH SELF-ORGANIZED M13 FILAMENTOUS PHAGE

DEVELOPING HYDROGELS WITH SELF-ORGANIZED M13 FILAMENTOUS PHAGE

December 2018

By:
AZADEH PEIVANDI, M.SC.

A Thesis Report
Submitted to the stream of Chemical Engineering
in Partial Fulfillment of the Requirements for the Degree of
Masters in Applied Science in Chemical Engineering
McMaster University
Fall 2018

McMaster
University
ENGINEERING

CHEMICAL ENGINEERING, ENGINEERING

Masters in Applied Science in Chemical Engineering
McMaster University. Hamilton Ontario

TITLE: Developing Hydrogels with M13 Filamentous Phage

AUTHOR: Azadeh Peivandi

SUPERVISOR: Dr. Zeinab Hosseini-Doust

(Chemical Engineering, Faculty of Engineering)

NUMBER OF PAGES: 56 & ix

Lay Abstract

Filamentous phage are viruses that infect bacteria. These bio-filaments are $\sim 1 \, \mu m$ long, 6-8 nm in diameter and can propagate themselves by infecting bacteria. This means one bio-filament can make 300-1000 particles only by infecting a bacterial host, a characteristic that drastically increases their utility over synthetic filamentous nanomaterial. Filamentous phage can be readily genetically engineered to express foreign receptors on their surface. In this thesis, I demonstrate how these bio-filaments can self-organize at high concentrations and can be crosslinked to make hydrogels that can adsorb up to 12 times their weight in water. These hydrogels can also heal themselves if broken or cut and exhibit autofluorescence, which are very useful properties for hydrogels used for biomedical applications. We further demonstrate that adding small proteins to the bio-filaments can expand the range of hydrogel formation, to the extent that even low concentrations of bio-filament can form hydrogels.

Abstract

Bacteriophages (phages) are bacterial viruses. Phages offer remarkable diversity and can be found in many shapes and sizes; however, what they all have in common is that they are made of protein nano-shells that encase their genome (DNA or RNA). In other words, phages are proteinous bionanoparticles. In this work, we use the filamentous phage M13. M13 is a simple virus with a high aspect ratio. It has 11 genes and only 5 structural proteins. The phage filament is almost entirely made of 2700 copies of pVIII, the major coat protein, and is capped off on one end by five copies each of the proteins pIII and pVI, while the opposite end displays five copies each of the proteins pVII and pIX. M13 phage can be genetically engineered to display certain peptides with affinity toward cancer cells, specific tissue, or even minerals and polymers. These filaments can further self-organize to form liquid crystals at high concentrations. All these properties make M13 a unique building block for the bottom up synthesis of advanced bioactive material.

The objective of my proposed research is to develop hydrogels using M13 phage. Hydrogels can absorb large quantities of water without dissolving. They mark a breakthrough in the field of biomaterials, owing to their high water content, porosity and soft consistency. I crosslinked M13 at liquid crystalline concentrations using glutaraldehyde. The resulting hydrogels were characterized for swelling and mechanical properties. These hydrogels exhibited self-healing and autofluorescence properties. In addition, I demonstrated that M13 can from self-healing hydrogels at lower concentrations by adding the small globular protein, BSA.

The developed M13 hydrogels mark the first step in the development of *bioactive* hydrogels that could be utilized to direct cell destiny and genuinely mimic the natural tissue.

Acknowledgements

Table of Contents

List of Figures

Declaration of Academic Achievement

The experiments reported in this thesis have been designed by my supervisor and carried out by myself, independently. Furthermore, I independently carried out all the troubleshooting experiments as designed by my supervisor. Phage propagation, purification and concentration for Chapter 2 was mainly performed by Randi Mahabir (author on my manuscripts). Electron micrographs were taken by Lei Tian (PhD student); the samples were all prepared by me. I performed data analysis independently and the first draft of all figures have been prepared by myself after being designed by my supervisor. The final form of the figures was edited by my supervisor. The text was written jointly by myself and my supervisor.

Chapter 1 – Introduction

1. Introduction to hydrogels

1.1. What is a hydrogel

Hydrogels are three-dimensional, *cross-linked* networks of hydrophilic polymers (homopolymers or copolymers) that are able to retain a large amount of water (>20% of their dry weight) or biological fluid without dissolving.[1] The crosslinked structure gives the hydrogels physical integrity as well as thermodynamic compatibility with water, which allows them to swell in aqueous media without dissolving.[2] Capillary interactions, osmotic and hydration forces are responsible for the water sorption properties.[3] For the same building blocks, changing the structure (the polymerization method) and number of crosslinks will change the equilibrium water content of a hydrogel.[4][4] Hydrogels can be made into different shapes by crosslinking of aqueous solutions/colloidal suspensions in suitable molds.[4]

Although natural hydrogels like agar and chitosan have been known for a long time, the first synthetic hydrogels (crosslinked glycomethacrylates) were introduced by Wichterle and Lim in 1960.[4] The authors presented hydrogels as a more physiologically favorable form of "plastic" because of structural similarity with tissue due to soft consistency and high levels of hydration as well as permeability to metabolites.[4] Hydrogel building blocks have since expanded beyond glycomethacrylates, and now constitute a wide range of synthetic and natural polymers as well as nanoparticles and nanocrystals.

1.2. Hydrogel building blocks

Hydrogels are two component systems: a hydrophilic, insoluble, three-dimensional network polymer, and water.[3] These two component systems are insoluble in water due to the presence of chemical and/or physical crosslinks (tie-points, junctions).[5] Furthermore, unlike other dispersed systems such as emulsions or suspensions, these two components are completely interpenetrating and continuous, therefore it is not possible to differentiate between a continuous and a dispersed phase.[3]

1.3. Hydrogel classification

Hydrogels may be classified depending on the source of the constituting polymers (natural, synthetic or hybrid),[2] based on the nature of the side groups of the constituting polymers (neutral or ionic),[5] according to their mechanical and structural characteristics (affine or phantom networks),[6] based on the physical structure of the networks (amorphous, semi crystalline, hydrogen-bonded structures, super molecular structures and hydrocolloidal aggregates),[5] or based on the physical state of the gel (solid, semi-solid, or liquid).[2] Hydrogels may additionally be classified based on their cross-linking preparative route.[1] Hydrogel networks may be physically crosslinked (repetitive freeze-thaw cycles,[7-9] stereocomplex formation,[10] ionic interactions, heat-induced[11,12]) or chemically crosslinked (chemical[13]or radiation grafting[14], radical polymerization,[15-17] condensation reactions,[18,19] enzymatic reaction,[20] high-energy γ or electron beam radiation[21,22]). The method of cross linking will affect the physical and mechanical properties of the hydrogel as well as how it responds to its surrounding environment. Due to high stability of covalent bonding resulting by chemical crosslinking, chemically crosslinked gels generally exhibit higher mechanical strength as well as physical integrity.[6,23,24] **Figure 1.1** shows a schematic representation of the various hydrogel cross-linking methods.[25]
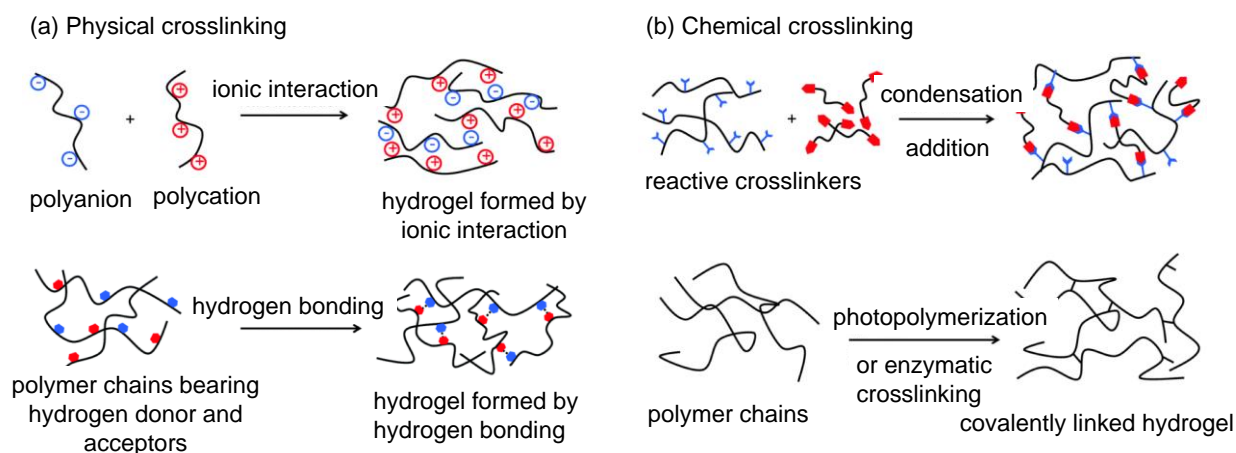
Figure 1.1. schematic representations of polymeric hydrogels formed by (a) physical gelation and (b) chemical gelation (reproduced with permission from reference 25).

1.4. Swelling behavior of hydrogels

The polymeric chain networks in a hydrogel interact with water or biological fluids through capillary, osmotic, and hydration forces, causing absorption of water and swelling.[1] Swelling ratio depends on the magnitude of these opposing effects that are affected by some inherent properties of the hydrogel, including internal transport, diffusion characteristics, and mechanical strength.[2]

Hydrogels may also show a swelling behavior dependent on the external environment. Physiologically-responsive hydrogels, for example, are hydrogels where polymer complexes can be broken or the network can be swollen as a result of the changing the external environment.[26] These systems may show drastic changes in their swelling ratio with physiological fluids and under changing pH, ionic strength, temperature and electromagnetic radiation.[26] Swelling behavior is quantified using the weight equilibrium swelling ratio, q, defined as weight of swollen matrix, W_s, per unit weight of dry polymer matrix, W_d: $q = \frac{W_s}{W_d}$

1.5. Application of hydrogels in biomedical engineering

Being soft, hydrated, hydrogels have found many applications in biomedical engineering, including contact lenses, wound dressing, drug delivery system, tissue engineering scaffolds, and hygiene products.[27]

Perhaps one of the areas that has garnered the most research interest is the use of hydrogels for tissue engineering (*e.g.,* linings for artificial hearts, materials for artificial skin, scaffolds for artificial organs) and drug delivery system. Hydrogels offer the possibility for controlled, sustained, and/or trigger responsive release, all of which are highly desired properties for drug delivery systems.[26] Furthermore, the high porosity of hydrogels allows drugs to be loaded and then released. These materials can be designed via crosslinking chemistry to respond to a number of physiological stimuli present in the body, such as pH,[28] ionic strength,[29] magnetic field,[30] and temperature.[31] Porosity can further be adjusted by controlling the cross-linking density.[32] Hydrogels containing large pores can also accommodate proliferation of living cells.[33] Hydrogels used in tissue engineering are usually required to be biodegradable.[34] These hydrogels can be impregnated with growth factors or

incorporate cell membrane receptor peptide ligands to stimulate adhesion and growth of cells.[35]

Soft contact lenses are one of the most notable commercialized applications of hydrogels.[27] Silicon hydrogels lenses have shown high oxygen permeability and comfortable fit.[36] These hydrogels have 95% luminous transmittance,[37,38] refractive index of 1.3,[39] sufficient oxygen permeability (35 Dk for the open eye and 125 Dk for the closed eye),[40] wettability and permeability to water (contact angle=25),[41] stability, good mechanical properties, and biocompatibility.

Wound dressings are another example of successfully commercialized hydrogels. Hydrogels can be designed to have good oxygen permeability and be supplied completely sterile. These characteristics combined with the hydrated nature of the hydrogel and absorb excess exudate make hydrogels ideal for wound treatment. Hydrogels are also suitable for dry wounds, this is where current wound dressings fall short.[42] Oxygen permeability is particularly important for pressure sores, leg ulcers, surgical and necrotic wounds, lacerations and burns.[43] **Figure 1.2** shows some examples of commercialized hydrogels.

Figure 1.2. Examples of commercialized hydrogel products. (a) Kendall Dermacea Aquaflo Hydrogel Wound Dressing; (b) P-DERM® Hydrogel Adhesives; (c) Soft contact lenses; (d) Most disposable baby diapers use sodium polyacrylate hydrogels.

2. Protein hydrogels

The building blocks of hydrogels are not limited to synthetic polymers. Natural polymers such as cellulose,[44] starch,[45] collagen,[46] silk,[47] and chitosan[48] have been reported to form hydrogels. Natural polymers are biodegradable and biocompatible by nature and they do not release toxic materials upon degradation. Proteins and peptides are a special class of natural polymers (with the monomer building blocks being amino acids). Proteins offer several

functional groups that make them amenable to a range of chemical reactions, allowing for chemical crosslinking, loading of different drugs, and trigger-responsive release.[49]

Peptides are amino acid sequences with less than 50 amino acids. Under specific conditions various peptide-based systems can self-assemble into fibrillar structures, which in turn associate and/or entangle to form hydrogels.[50] Proteins are basically large peptides; because of their large structure, they can have secondary, tertiary and quaternary structure. Proteins and peptides can interact specifically with other proteins, DNA and RNA, and even minerals and ions.[51] Therefore, the added advantage of using proteins and peptides to make hydrogels is the possibility of having specific interaction designed into the building blocks of the hydrogel.

Glutaraldehyde or water-soluble carbodiimides are widely used as protein cross-linkers.[52] Proteins such as collagen,[46] gelatin,[53] bovine serum albumin (BSA),[54] and human serum albumin (HSA)[55] have been used and make hydrogels. Despite toxicity of glutaraldehyde, glutaraldehyde-crosslinked hydrogels have been shown to be biocompatible according to the *in vitro* cytotoxicity test and *in vivo* biocompatibility experiments.[54,56]

3. Phage hydrogels

3.1. Structure and chemistry of filamentous phage

Bacteriophages, or phage for short, are viruses that infect bacteria. Phages offer remarkable diversity in terms of both genomic sequence and physical appearance and can be found in many shapes and sizes (**Figure 1.3**);[57] however, what they all have in common is that they are made of protein shells that encase their genome (DNA or RNA). This means phages are essentially proteinous nanoparticles. The chemistry of the bacteriophage protein coat can be controlled with atomic precision via genetic engineering, making them superior to synthetic nanoparticles.
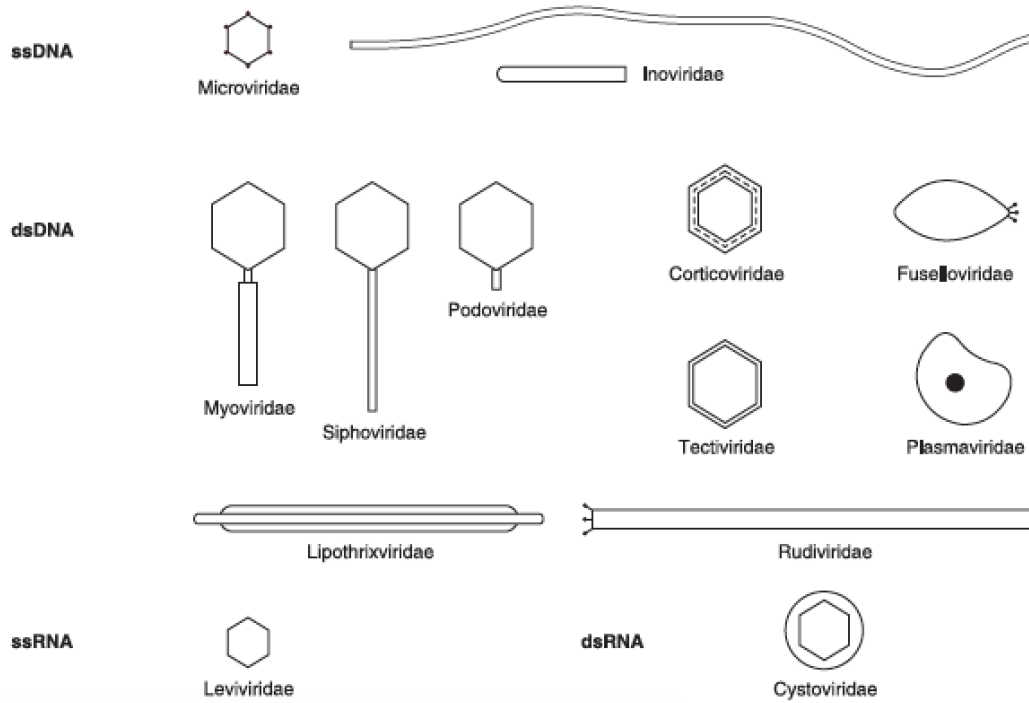
Figure 1.3. *Schematic representation of major phage groups (reproduced with permission from reference 57).*

Filamentous phages are a special class of bacteriophages that are in the form of large aspect ratio protein filaments that encase the phage circular DNA genome. These phages do not reproduce by lysing bacteria; instead, they are secreted into the environment without killing the host.[58] The lysogenic cycle for these phages contains 4 steps; attachment: Proteins in the "tail" of the phage bind to a specific receptor on the surface of the bacterial cell. Entry: The phage injects its double-stranded DNA genome into the cytoplasm of the bacterium. DNA recombines with a particular region of the bacterial chromosome. This causes the phage DNA to be integrated into the chromosome. DNA copying and protein synthesis: Phage DNA is copied, and phage genes are expressed to make proteins, such as capsid proteins. Assembly of new phage: Capsids assemble from the capsid proteins and are stuffed with DNA to make lots of new phage particles.[58]

The most well-studied phages in this family include *f1*, *fd* and M13.[58] Filamentous phages offer properties that present them as unique building blocks for the bottom-up synthesis of advanced materials.

Phage M13 has been extensively used for the bottom-up synthesis of functional materials, ranging from tissue engineering scaffolds to batteries.[59] M13 is a simple virus; it has 11 genes and only 5 structural proteins. The phage filament is almost entirely made of 2700 copies of pVIII, the major coat protein, and is capped off on one end by five copies each of the proteins pIII and pVI, while the opposite end displays five copies each of the proteins pVII and pIX (**Figure 1.4**). Wild-type M13 is 0.88 μm long and has a diameter D=6.6 nm, and molecular weight M=1.6×10^7 g/mol.[60] At pH 8.2, M13 has 2.4 negative charges. This translates to a linear charge density of 10 charges/nm, which is high enough to condense free ions onto the virus.

Filamentous phages have a unique ability to package very long or short DNA segments and filament length scales linearly with genome size. Using molecular cloning, viruses as short as 50 nm[61] and as long as 8000 nm[62] have been made. M13 can be genetically engineered to display certain peptides with affinity toward cancer cells, specific tissue, or even minerals. M13 is also at the center of the Nobel Prize winning research, phage display. The first paper on this method was published in 1985 by George Smith.[63] Phage display allows for fast and efficient screening of peptides that bind to proteins, enzymes, cells, or minerals. This technology, however, is not the subject of the current thesis. In addition to genetic modification, M13 is also amenable to a range of chemical reactions, which will further expand the range of surface functionalities for M13 (**Figure 1.5**).[64,65]
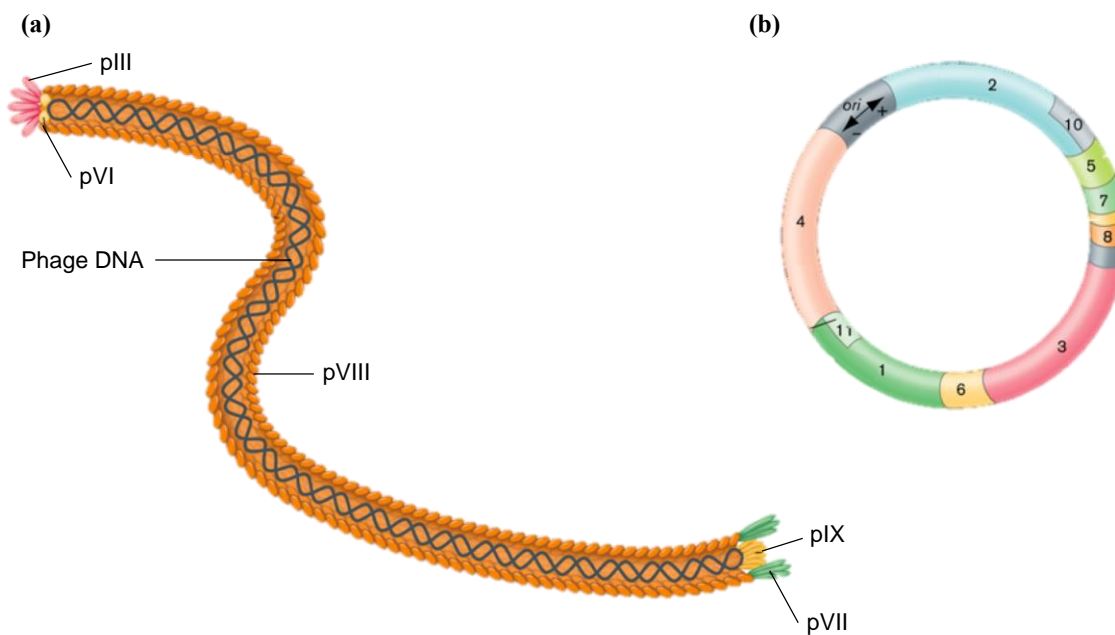
Figure 1.4. *(a) schematic representation of M13 bacteriophage with its single stranded DNA and capsid proteins. (b) A map of the circular phage genome showing the 11 genes (reproduced with permission from reference 65).*
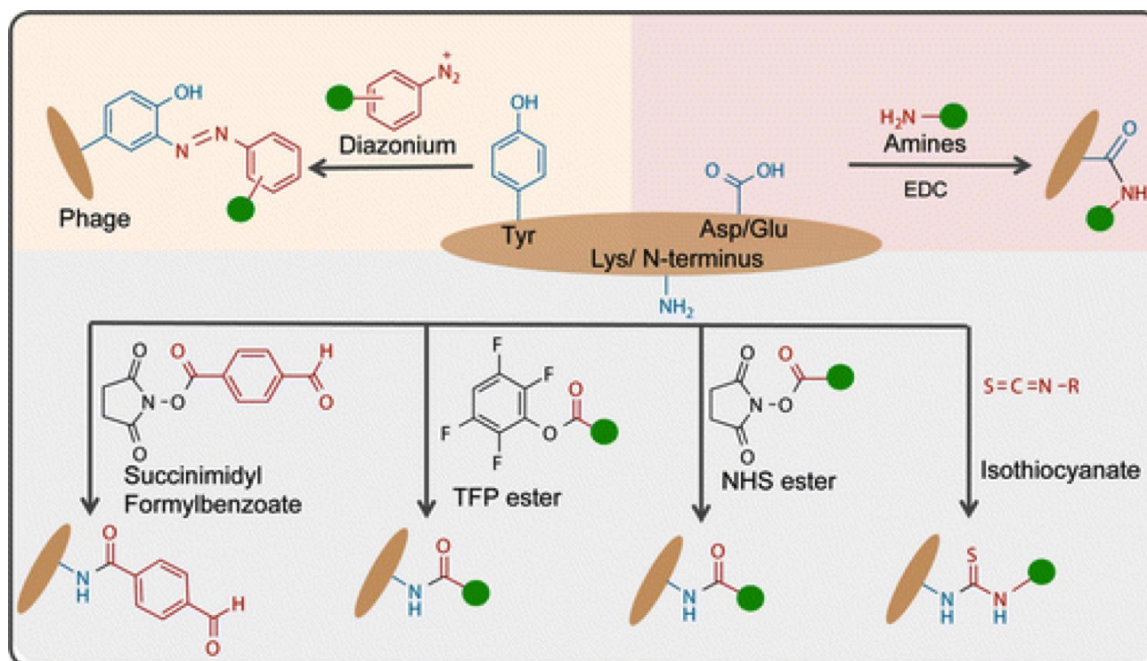
Figure 1.5. *A summary chemical reactions for the outer membrane proteins of M13 phage (reproduced with permission from reference 64).*

3.2. Self-organized structures of filamentous phage

M13 filaments self-organize into liquid crystalline phase at high concentrations. Liquid crystals are comprised from rod-shaped molecules or colloidal particles. At low concentrations, these rod-like molecules are disordered and randomly oriented (*i.e.,* isotropic phase). At higher particle concentrations, all rods are aligned along one particular axis, forming a nematic liquid crystal (**Figure 1.6a**).[60] Increasing the particle concentration leads to more ordered phases, namely a smectic phase with a long-range orientational order and 1D quasi-long-range positional order. The liquid crystalline phase of filamentous phage was first characterized by Don Marvin *et al* in 1973.[66] A unique feature of the rod-like viruses is that some of them, such as the M13 and *fd* viruses, can form chiral nematic liquid crystal phases.[67] In a chiral nematic phase, the long axis of the rod-like virus arranges in a helical way around a director, resulting in stripe-like fingerprints (**Figure 1.6b**). Filamentous viruses form lyotropic or concentration-induced liquid crystals.[67] M13 forms an isotropic phase at low concentrations ($5\,{mg}/{mL}$); at higher concentrations, it forms nematic phase (14-22 ${mg}/{mL}$) and chiral nematic phase (28-76 ${mg}/{mL}$).[68] These concentrations may change under different pH and ionic strengths. The liquid crystal phase is usually visualized in a confined environment (capillary tubes) and at low temperatures ($\sim4°C$). Phage liquid crystals have been used to investigate the mechanistic details of chiral nematic liquid crystals formed by colloidal particles. Furthermore, these ordered structures have been used to form highly ordered films that are then utilized as scaffolds for mineralizing metal ions or other elements[69] or for making biosensing surfaces.[70,71] Based on my literature review, most M13 hydrogels reported to date have been formed in concentration ranges representative of a liquid crystal phase.
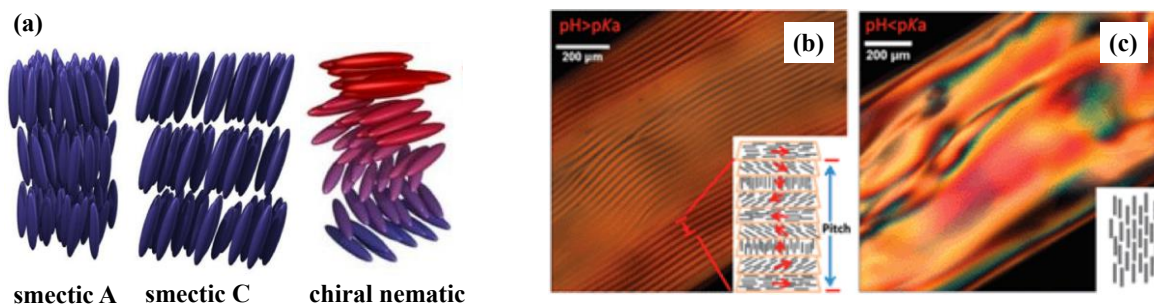
Figure 1.6. *(a) Schematic illustration of rods in an smectic and nematic liquid crystal phase.[72] (b) Typical texture of a chiral nematic phase of M13 phage, observed with polarization microscopy. Dark lines correspond to regions where the rods are perpendicular to the plane of the paper and bright lines correspond to regions where rods are in the plane of paper.[73] (c) pure nematic phase of M13 (reproduced with permission from references 72 & 73).*

3.3. Previous reports on phage hydrogels

The use of crosslinked M13 dates back to the first years of discovery of the phage display method. In 1998, George Smith crosslinked *fd* phage ($>10^{13}$ virions/mL) with NHS-dextran chemistry to make an "insoluble" hydrophilic aggregate that was then pelleted by low-speed centrifugation.[74] This aggregate was stable in acid buffers (pH down to 2.2).[74] Furthermore, when phage displayed a peptide (via genetic modification), the aggregate served as an effective affinity matrix for absorbing and affinity-purifying antibodies that could specifically bind the expressed peptide.[74] They reported the pellet to be turbid in 0.15 M NaCl but to transform into a loose, gelatinous, nearly transparent pellet in water with a volume up to 25 times larger.[74] The same chemistry was used in 2004 for making a solid matrix with phage expressing RGD peptide.[75] When whole cell lysate from rat glioma cells was passed through the matrix, cell membrane components having strong affinity to the peptides expressed on phage surface were isolated.[75]

One of the first reports that used the term "hydrogel" for crosslinked M13 phage was published in 2008 by the Japanese Foundation for Cancer Research, where the authors coated a titanium surface with M13 (50 mg/mL crosslinked with 2% glutaraldehyde) displaying a titanium binding peptide and used the coated surface for growing mouse fibroblasts.[76] They, however, did not make any efforts to characterize the hydrogel.

A number of publications from Angela Belcher's lab at MIT also used crosslinked M13 phage (genetically modified to bind specific metals/polymers) to make phage "hydrogel" films that were then used as templates for nucleating titanium dioxide,[77] coating conductive polymers,[78] or binding Ruthenium (Ru) or cobalt ferrite (CoFe2O4),[79] quantum dots,[80] and gold.[81] Hydrogels were prepared by exposing a layer of dried M13 on a substrate to 50% glutaraldehyde to crosslink M13 (**Figure 1.7a**),[77,78] spinning a concentrated M13 suspension into 2.5% glutaraldehyde,[80] ice templating (physical crosslinking) for aerogels,[79] or streptavidin-biotin interaction.[81] It is noteworthy that they also made 3D M13 networks (not claimed to be hydrogels) using other methods such as layer-by-layer assembly.[82]

Using a physical crosslinking strategy (mediated by salt induced electrostatic interactions) and in a collaborative effort, Renata Pasqualini's group at University of Texas developed M13 phage hydrogels that were crosslinked with gold nanoparticles (**Figure 1.7b,c**).[83] A genetic modification that increased the number of surface amine groups, hence the number of local positive charge, enhanced hydrogel stability.[84] These hydrogels were optically active, due to the presence of gold nanoparticles, and were demonstrated to have application in medical imaging.[83] When impregnated with magnetic nanoparticles, these hydrogels were used as levitating scaffold for 3D tissue culture (**Figure 1.7d**).[85] The same group further developed a hydrogel-based platform containing heat-sensitive liposomes for triggered drug delivery, multimodal imaging, and controlled release of therapeutic cargo.[86]
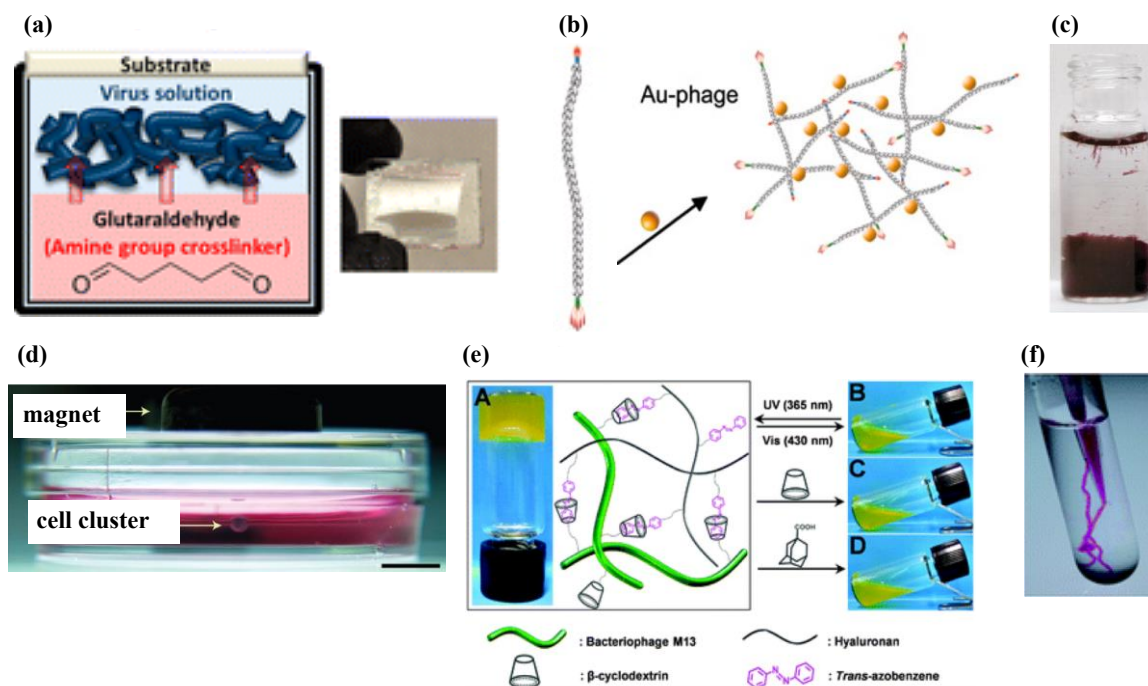
Figure 1.7. *(a) Schematic illustration of hydrogel formation via glutaraldehyde crosslinking of drop-cast phage film.[77](b) Strategy for Au assembly onto phage nanoparticles.[83] (c) Vial of gold–phage hydrogel.[83] (d) Human glioblastoma cells (lower arrow) treated with magnetic iron oxide-containing hydrogel held at the air–medium interface by a magnet.[85] (e) Illustration of the light- and chemical-responsiveness of the hybrid M13 hydrogels.[87] (f) hydrogel forms instantly when the polymer grafted virus in the sol state was injected into the aqueous solution at 37 °C.[88] (reproduced with permission from reference 77, 83, 85, 87, 88)*

Another physical crosslinking strategy involves grafting end-functionalized phenylboronic acid containing PNIPAM random copolymers to M13 phage.[88] The gelation behavior was then regulated by temperature, pH or diol-containing compounds such as glucose.[88] In another instance of combining polymers and M13 phage, a light- and chemical-responsive supramolecular hydrogel of bacteriophage M13 and hyaluronan was made utilizing the chemical interaction between β-cyclodextrin and trans-azobenzene moieties (Figure 7e).[87]

Other notable examples include a report from Tokyo Institute of Technology where antigen-displaying M13 was crosslinked using antibody modified gold nanoparticles.[89] These hydrogels were also cast into gel strings by injecting into a 5% glutaraldehyde solution, thus combining physical and chemical crosslinking (Figure 7f).[90]

Hybrid hydrogels were also made by physically cross-linked gelatin and liquid-crystalline

M13 phages,[91] or physically crosslinking phages displaying hydroxyapatite (HA)-binding peptides with gelatin (used for controlled-release of HA antibodies).[92]

There have been numerous reports on viruses and phage imbedded in natural polymers that gel independent of the presence of phage, such as alginate, agar,[93] and gelatin,[92] or biodegradable synthetic hydrogels, such as PEG-maleimide hydrogels.[94] The motivation for making phage-imbedded hydrogels is mainly to make antibacterial hydrogels and these hydrogels should not be confused with hydrogels that are formed by self-organized phage because there have been no effort to confirm the effect of phage on gelation or hydrogel properties.

4. Aim and hypothesis

The aim of my thesis was to develop hydrogels with filamentous phage, M13. The long-term goal of this research is to develop hydrogels that are bioactive and can be tailored to interact actively with the surrounding environment. To do so, however, requires us to develop the methods and fundamental knowledge related to phage hydrogels.

The current thesis was designed to test two major hypotheses:

-   At high enough concentrations, where M13 exhibits concentration-mediated self-organization, M13 can be cross-linked into a single-component, free-standing hydrogel.

-   The range of M13 hydrogel formation can be expanded (beyond self-organization range) by supplementing the system with small globular molecules (in this case bovine serum albumin).

During the course of this work, we encountered several interesting properties for M13 hydrogels, namely autofluorescence and self-healing properties. These properties, along with the ability to express foreign peptides on the surface of M13, make M13 hydrogels highly attractive functional materials that can find applications in a range of biomedical and environmental applications.

5. Contributions to knowledge

This work resulted in the development of fundamental knowledge related to M13 self-organization and M13 hydrogels that will be reported in the form of two manuscripts (I am the first author on both manuscripts):

1- Self-organizing bundles of filamentous phage form hierarchically-structured, self-healing, fluorescent hydrogels (Chapter 2), to be submitted to *ACS Materials & Interfaces*

2- Synergistic action between filamentous phage and globular protein forms self-healing bioactive hydrogels (Chapter 3), to be submitted to *Biomacromolecules*

The developed insight and knowledge can be applied for designing bioactive hydrogel coatings for other indwelling medical devices, as well as for designing bioactive tissue engineering scaffolds, wound dressings and cell therapy vehicles. The applications of these novel hydrogels are not limited to biomedical engineering, they can also be used in environmental engineering for decontaminating contaminated water.

6. References

1   Varaprasad, K., Raghavendra, G. M., Jayaramudu, T., Yallapu, M. M. & Sadiku, R. A mini review on hydrogels classification and recent developments in miscellaneous applications. *Materials Science and Engineering: C* **79**, 958-971, (2017).

2   Buwalda, S. J. *et al.* Hydrogels in a historical perspective: From simple networks to smart materials. *J. Controlled Release* **190**, 254-273, (2014).

3   Roorda, W. E., BoddÉ, H. E., de Boer, A. G. & Junginger, H. E. Synthetic hydrogels as drug delivery systems. *Pharm. Weekbl.* **8**, 165-189, (1986).

4   Wichterle, O. & LÍM, D. Hydrophilic Gels for Biological Use. *Nature* **185**, 117, (1960).

5   Peppas, N. A., Bures, P., Leobandung, W. & Ichikawa, H. Hydrogels in pharmaceutical formulations. *Eur. J. Pharm. Biopharm.* **50**, 27-46, (2000).

6   Akagi, Y., Gong, J. P., Chung, U.-i. & Sakai, T. Transition between Phantom and Affine Network Model Observed in Polymer Gels with Controlled Network Structure. *Macromolecules* **46**, 1035-1040, (2013).

7   Hassan, C. M. & Peppas, N. A. in *Biopolymers · PVA Hydrogels, Anionic Polymerisation Nanocomposites*   37-65 (Springer Berlin Heidelberg, 2000).

8   Plieva Fatima, M. *et al.* Pore structure of macroporous monolithic cryogels prepared from poly(vinyl alcohol). *J. Appl. Polym. Sci.* **100**, 1057-1066, (2006).

9   Jayaramudu, T., Li, Y., Ko, H.-U., Shishir, I. R. & Kim, J. Poly(acrylic acid)-Poly(vinyl alcohol) hydrogels for reconfigurable lens actuators. *International Journal of Precision Engineering and Manufacturing-Green Technology* **3**, 375-379, (2016).

10   Hideto, T. Poly(lactide) Stereocomplexes: Formation, Structure, Properties, Degradation, and Applications. *Macromol. Biosci.* **5**, 569-597, (2005).

11   Aoki, H., Al-Assaf, S., Katayama, T. & Phillips, G. O. Characterization and properties of Acacia senegal (L.) Willd. var. senegal with enhanced properties (Acacia (sen) SUPER GUM™): Part 2—Mechanism of the maturation process. *Food Hydrocolloids* **21**, 329-337, (2007).

12   Aoki, H. *et al.* Characterization and properties of Acacia senegal (L.) Willd. var. Senegal with enhanced properties (Acacia (sen) SUPER GUM™): Part 5. Factors affecting the emulsification of Acacia senegal and Acacia (sen) SUPER GUM™. *Food Hydrocolloids* **21**, 353-358, (2007).

13   Athawale, V. D. & Lele, V. Graft copolymerization onto starch. II. Grafting of acrylic acid and preparation of it's hydrogels. *Carbohydr. Polym.* **35**, 21-27, (1998).

14   Said, H. M., Abd Alla, S. G. & El-Naggar, A. W. M. Synthesis and characterization of novel gels based on carboxymethyl cellulose/acrylic acid prepared by electron beam irradiation. *React. Funct. Polym.* **61**, 397-404, (2004).

15   Jayaramudu, T. *et al.* 5-Fluorouracil encapsulated magnetic nanohydrogels for drug-delivery applications. *J. Appl. Polym. Sci.* **133**, (2016).

16   Varaprasad, K. *et al.* Hydrogel–silver nanoparticle composites: A new generation of antimicrobials. *J. Appl. Polym. Sci.* **115**, 1199-1207, (2009).

17   Jayaramudu, T., Raghavendra, G. M., Varaprasad, K., Sadiku, R. & Raju, K. M. Development of novel biodegradable Au nanocomposite hydrogels based on wheat: For inactivation of bacteria. *Carbohydr. Polym.* **92**, 2193-2200, (2013).

18   de Nooy, A. E. J., Capitani, D., Masci, G. & Crescenzi, V. Ionic Polysaccharide Hydrogels via the Passerini and Ugi Multicomponent Condensations: Synthesis, Behavior and Solid-State NMR Characterization. *Biomacromolecules* **1**, 259-267, (2000).

19   de Nooy, A. E. J., Masci, G. & Crescenzi, V. Versatile Synthesis of Polysaccharide Hydrogels Using the Passerini and Ugi Multicomponent Condensations. *Macromolecules* **32**, 1318-1320, (1999).

20   Sperinde, J. J. & Griffith, L. G. Synthesis and Characterization of Enzymatically-Cross-Linked Poly(ethylene glycol) Hydrogels. *Macromolecules* **30**, 5255-5264, (1997).

21   Zhao, L. *et al.* Synthesis of antibacterial PVA/CM-chitosan blend hydrogels with electron beam irradiation. *Carbohydr. Polym.* **53**, 439-446, (2003).

22   Zhai, M., Yoshii, F., Kume, T. & Hashim, K. Syntheses of PVA/starch grafted hydrogels by irradiation. *Carbohydr. Polym.* **50**, 295-303, (2002).

23   Rowley, J. A., Madlambayan, G. & Mooney, D. J. Alginate hydrogels as synthetic extracellular matrix materials. *Biomaterials* **20**, 45-53, (1999).

24   Akhtar, M. F., Hanif, M. & Ranjha, N. M. Methods of synthesis of hydrogels, A review. *Saudi Pharmaceutical Journal* **24**, 554-559, (2016).

25   Ghobril, C. & Grinstaff, M. W. The chemistry and engineering of polymeric hydrogel adhesives for wound closure: a tutorial. *Chem. Soc. Rev.* **44**, 1820-1835, (2015).

26   Peppas, N. A. Physiologically Responsive Hydrogels. *J. Bioact. Compatible Polym.* **6**, 241-246, (1991).

27   Caló, E. & Khutoryanskiy, V. V. Biomedical applications of hydrogels: A review of patents and commercial products. *Eur. Polym. J.* **65**, 252-267, (2015).

28   Rizwan, M. *et al.* pH Sensitive Hydrogels in Drug Delivery: Brief History, Properties, Swelling, and Release Mechanism, Material Selection and Applications. *Polymers* **9**, 137, (2017).

29   Xiao, S. *et al.* Salt-Responsive Bilayer Hydrogels with Pseudo-Double-Network Structure Actuated by Polyelectrolyte and Antipolyelectrolyte Effects. *ACS Applied Materials & Interfaces* **9**, 20843-20851, (2017).

30   Li, Y. *et al.* Magnetic Hydrogels and Their Potential Biomedical Applications. *Adv. Funct. Mater.* **23**, 660-672, (2013).
31   Yan, H. *et al.* Thermo-reversible protein fibrillar hydrogels as cell scaffolds. *Faraday Discuss.* **139**, 71-84, (2008).
32   Calvino-Casilda, V. *et al.* Porosity Inherent to Chemically Crosslinked Polymers. Poly(N-vinylimidazole) Hydrogels. *The Journal of Physical Chemistry B* **112**, 2809-2817, (2008).
33   Nagaoka, S., Tanzawa, H. & Suzuki, J. Cell proliferation on hydrogels. *In Vitro Cell. Dev. Biol.* **26**, 51-56, (1990).
34   Kamath, K. R. & Park, K. Biodegradable hydrogels in drug delivery. *Adv. Drug Del. Rev.* **11**, 59-84, (1993).
35   Silva, A. K. A., Richard, C., Bessodes, M., Scherman, D. & Merten, O.-W. Growth Factor Delivery Approaches in Hydrogels. *Biomacromolecules* **10**, 9-18, (2009).
36   Kojima, T. *et al.* Effect of Controlled Adverse Chamber Environment Exposure on Tear Functions in Silicon Hydrogel and Hydrogel Soft Contact Lens Wearers. *Invest. Ophthalmol. Vis. Sci.* **52**, 8811-8817, (2011).
37   Zhou, Y., Cai, Y., Hu, X. & Long, Y. Temperature-responsive hydrogel with ultra-large solar modulation and high luminous transmission for "smart window" applications. *Journal of Materials Chemistry A* **2**, 13550-13555, (2014).
38   Osuagwu, U. L. & Ogbuehi, K. C. UV–vis light transmittance through tinted contact lenses and the effect of color on values. *Contact Lens and Anterior Eye* **37**, 136-143, (2014).
39   Patel, S., Alió, J. L. & Pérez-Santonja, J. J. Refractive Index Change in Bovine and Human Corneal Stroma before and after LASIK: A Study of Untreated and Re-treated Corneas Implicating Stromal Hydration. *Invest. Ophthalmol. Vis. Sci.* **45**, 3523-3530, (2004).
40   Hadassah, J. & Sehgal, P. A novel method to measure oxygen permeability and transmissibility of contact lenses. *Clinical and Experimental Optometry* **89**, 374-380, (2006).
41   Ketelson, H. A., Meadows, D. L. & Stone, R. P. Dynamic wettability properties of a soft contact lens hydrogel. *Colloids Surf. B. Biointerfaces* **40**, 1-9, (2005).
42   Ajji, Z., Othman, I. & Rosiak, J. M. Production of hydrogel wound dressings using gamma radiation. *Nuclear Instruments and Methods in Physics Research Section B: Beam Interactions with Materials and Atoms* **229**, 375-380, (2005).
43   Jones, A. & Vaughan, D. Hydrogel dressings in the management of a variety of wound types: A review. *Journal of Orthopaedic Nursing* **9**, S1-S11, (2005).
44   Mohammed, N., Grishkewich, N., Berry, R. M. & Tam, K. C. Cellulose nanocrystal–alginate hydrogel beads as novel adsorbents for organic dyes in aqueous solutions. *Cellulose*, (2015).
45   Xu, X. *et al.* Preparation and in vitro characterization of thermosensitive and mucoadhesive hydrogels for nasal delivery of phenylephrine hydrochloride. *Eur. J. Pharm. Biopharm.* **88**, 998-1004, (2014).
46   Olde Damink, L. H. H. *et al.* Glutaraldehyde as a crosslinking agent for collagen-based biomaterials. *J. Mater. Sci. Mater. Med.* **6**, 460-472, (1995).
47   Kim, U.-J. *et al.* Structure and Properties of Silk Hydrogels. *Biomacromolecules* **5**, 786-792, (2004).
48   Nieto-Suárez, M., López-Quintela, M. A. & Lazzari, M. Preparation and characterization of crosslinked chitosan/gelatin scaffolds by ice segregation induced self-assembly. *Carbohydr. Polym.* **141**, 175-183, (2016).

49   Krall, N., da Cruz, F. P., Boutureira, O. & Bernardes, G. J. L. Site-selective protein-modification chemistry for basic biology and drug development. *Nat. Chem.* **8**, 103, (2015).

50   Tang, C., Miller, A. F. & Saiani, A. Peptide hydrogels as mucoadhesives for local drug delivery. *Int. J. Pharm.* **465**, 427-435, (2014).

51   Andersen, A. *et al.* Protein–Mineral Interactions: Molecular Dynamics Simulations Capture Importance of Variations in Mineral Surface Composition and Structure. *Langmuir* **32**, 6194-6209, (2016).

52   Cheung, D. T. & Nimni, M. E. Mechanism of crosslinking of proteins by glutaraldehyde I: reaction with model compounds. *Connect. Tissue Res.* **10**, 187-199, (1982).

53   Bigi, A., Cojazzi, G., Panzavolta, S., Rubini, K. & Roveri, N. Mechanical and thermal properties of gelatin films at different degrees of glutaraldehyde crosslinking. *Biomaterials* **22**, 763-768, (2001).

54   Ma, X. *et al.* A Biocompatible and Biodegradable Protein Hydrogel with Green and Red Autofluorescence: Preparation, Characterization and In Vivo Biodegradation Tracking and Modeling. *Sci. Rep.* **6**, 19370, (2016).

55   Elmer, J., Cabrales, P., Wang, Q., Zhang, N. & Palmer, A. F. Synthesis and biophysical properties of polymerized human serum albumin. *Biotechnol. Prog.* **27**, 290-296, (2011).

56   Lai, J.-Y. Biocompatibility of Genipin and Glutaraldehyde Cross-Linked Chitosan Materials in the Anterior Chamber of the Eye. *International Journal of Molecular Sciences* **13**, 10970-10985, (2012).

57   Calendar, R. L. *The Bacteriophages*. second edn, (Oxford University Press, 2006).

58   Rakonjac, J. *Filamentous Bacteriophages: Biology and Applications*. (2012).

59   Lee, J. H. *et al.* Production of tunable nanomaterials using hierarchically assembled bacteriophages. *Nat. Protocols* **12**, 1999-2013, (2017).

60   Dogic, Z. & Fraden, S. Ordered phases of filamentous viruses. *Current Opinion in Colloid & Interface Science* **11**, 47-55, (2006).

61   Specthrie, L. *et al.* Construction of a microphage variant of filamentous bacteriophage. *J. Mol. Biol.* **228**, 720-724, (1992).

62   Marchi, A. N., Saaem, I., Vogen, B. N., Brown, S. & LaBean, T. H. Toward Larger DNA Origami. *Nano Lett.* **14**, 5740-5747, (2014).

63   Smith, G. P. Filamentous fusion phage: Novel expression vectors that display cloned antigens on the virion surface. *Science* **228**, 1315-1317, (1985).

64   Mohan, K. & Weiss, G. A. Chemically Modifying Viruses for Diverse Applications. *ACS Chem. Biol.* **11**, 1167-1179, (2016).

65   Slonczewski, J., L. & Foster, J., W. *Microbiology: An Evolving Science*. 2 edn, (Norton & Company Inc, 2010).

66   Lapointe, J. & Marvin, D. A. Filamentous Bacterial Viruses VIII. Liquid Crystals of fd. *Molecular Crystals and Liquid Crystals* **19**, 269-278, (1973).

67   Dogic, Z. & Fraden, S. Cholesteric Phase in Virus Suspensions. *Langmuir* **16**, 7820-7824, (2000).

68   Lee, S.-W., Mao, C., Flynn, C. E. & Belcher, A. M. Ordering of Quantum Dots Using Genetically Engineered Viruses. *Science* **296**, 892-895, (2002).

69   Lee, S. W., Lee, S. K. & Belcher, A. M. Virus-Based Alignment of Inorganic, Organic, and Biological Nanosized Materials. *Adv. Mater.* **15**, 689-692, (2003).

70   Lee, J. H. *et al.* Phage-Based Structural Color Sensors and Their Pattern Recognition Sensing System. *ACS Nano* **11**, 3632-3641, (2017).

71   Sawada, T. *et al.* Filamentous Virus-based Assembly: Their Oriented Structures and Thermal Diffusivity. *Sci. Rep.* **8**, 5412, (2018).

72   Mitov, M. Cholesteric liquid crystals in living matter. *Soft Matter* **13**, 4176-4209, (2017).

73   Cao, J., Liu, S., Xiong, J., Chen, Y. & Zhang, Z. Stimuli responsive chiral liquid crystal phases of phenylboronic acid functionalized rodlike viruses and their interaction with biologically important diols. *Chem. Commun.* **50**, 10402-10405, (2014).

74   Smith, G. P., Petrenko, V. A. & Matthews, L. J. Cross-linked filamentous phage as an affinity matrix. *J. Immunol. Methods* **215**, 151-161, (1998).

75   Samoylova, T. I. *et al.* Phage matrix for isolation of glioma cell membrane proteins. *BioTechniques* **37**, 254-260, (2004).

76   Kashiwagi, K. & Shiba, K. in *2008 International Symposium on Micro-NanoMechatronics and Human Science.* 392-395.

77   Chen, P.-Y. *et al.* Versatile Three-Dimensional Virus-Based Template for Dye-Sensitized Solar Cells with Improved Electron Transport and Light Harvesting. *ACS Nano* **7**, 6563-6574, (2013).

78   Chen, P.-Y. *et al.* Assembly of Viral Hydrogels for Three-Dimensional Conducting Nanocomposites. *Adv. Mater.* **26**, 5101-5107, (2014).

79   Jung, S. M., Qi, J., Oh, D., Belcher, A. & Kong, J. M13 Virus Aerogels as a Scaffold for Functional Inorganic Materials. *Adv. Funct. Mater.* **27**, 1603203, (2017).

80   Chiang, C.-Y. *et al.* Weaving Genetically Engineered Functionality into Mechanically Robust Virus Fibers. *Adv. Mater.* **19**, 826-832, (2007).

81   Lee, S.-W., Lee, S. K. & Belcher, A. M. Virus-Based Alignment of Inorganic, Organic, and Biological Nanosized Materials. *Adv. Mater.* **15**, 689-692, (2003).

82   Courchesne, N.-M. D. *et al.* Assembly of a Bacteriophage-Based Template for the Organization of Materials into Nanoporous Networks. *Adv. Mater.* **26**, 3398-3404, (2014).

83   Souza, G. R. *et al.* Networks of gold nanoparticles and bacteriophage as biological sensors and cell-targeting agents. *Proceedings of the National Academy of Sciences* **103**, 1215-1220, (2006).

84   Souza, G. R. *et al.* Bottom-Up Assembly of Hydrogels from Bacteriophage and Au Nanoparticles: The Effect of Cis- and Trans-Acting Factors. *PLoS One* **3**, e2242, (2008).

85   Souza, G. R. *et al.* Three-dimensional tissue culture based on magnetic cell levitation. *Nature Nanotechnology* **5**, 291, (2010).

86   Hosoya, H. *et al.* Integrated nanotechnology platform for tumor-targeted multimodal imaging and therapeutic cargo release. *Proceedings of the National Academy of Sciences* **113**, 1877-1882, (2016).

87   Chen, L., Zhao, X., Lin, Y., Su, Z. & Wang, Q. Dual stimuli-responsive supramolecular hydrogel of bionanoparticles and hyaluronan. *Polymer Chemistry* **5**, 6754-6760, (2014).

88   Cao, J., Liu, S., Chen, Y., Shi, L. & Zhang, Z. Synthesis of end-functionalized boronic acid containing copolymers and their bioconjugates with rod-like viruses for multiple responsive hydrogels. *Polymer Chemistry* **5**, 5029-5036, (2014).

89   Sawada, T., Kang, S., Watanabe, J., Mihara, H. & Serizawa, T. Hybrid Hydrogels Composed of Regularly Assembled Filamentous Viruses and Gold Nanoparticles. *ACS Macro Lett.* **3**, 341-345, (2014).

90   Sawada, T. *et al.* Regular assembly of filamentous viruses and gold nanoparticles by specific interactions and subsequent chemical crosslinking. *Polym. J.* **46**, 511, (2014).

91   Sawada, T., Otsuka, H., Yui, H. & Serizawa, T. Preparation and characterization of hybrid hydrogels composed of physically cross-linked gelatin and liquid-crystalline filamentous viruses. *Polym. Bull.* **72**, 1487-1496, (2015).

92   Sawada, T., Yanagimachi, M. & Serizawa, T. Controlled release of antibody proteins from liquid crystalline hydrogels composed of genetically engineered filamentous viruses. *Materials Chemistry Frontiers* **1**, 146-151, (2017).

93   Balcão, V. M. *et al.* Carbohydrate Hydrogels with Stabilized Phage Particles for Bacterial Biosensing: Bacterium Diffusion Studies. *Appl. Biochem. Biotechnol.* **172**, 1194-1214, (2014).

94   Johnson, C., Dinjaski, N., Prieto, M. A. & Garcia, A. J. Controlled bacteriophage release from poly(ethylene glycol) hydrogels significantly reduces infection in a bone implant-associated infection model. *Frontiers in Bioengineering and Biotechnology*, (2016).

Chapter 2 – Structure and Properties of Filamentous Phage Hydrogels

1. Abstract

Bacteriophages (bacterial viruses) are essentially proteinous bionanoparticles, superior to any and all synthetic nanoparticles as building blocks for bottom-up synthesis of multifunctional materials with advanced properties, because they possess a protein coat, the composition of which can be controlled with atomic precision via genetic engineering. We report hierarchically-structured hydrogels of self-organized M13 bundles composed of hundreds of M13 nanofilaments that impart both long range and micron scale order, visible in electron micrographs of the crosslinked state, and can adsorb up to 15× their weight in water. We further demonstrate that these hierarchical hydrogels of M13 exhibit advanced properties at room temperature, namely self-healing under biological conditions, autofluorescence in three channels, and biological activity in the crosslinked state towards their host bacterial cells. The filamentous phage M13, which claimed fame through the powerful phage display technology, has garnered significant attention in the past decade for the development of functional materials, ranging from tissue engineering scaffolds to batteries. Our investigation, reveals the ability of these nano-filaments to self-organized into hierarchically-structured soft matter, highlighting the power of self-organized M13 structures as building blocks for bottom-up synthesis.

2. Introduction

Filamentous bacteriophages (bacterial viruses) of *E. coli* (f1, M13 and fd) have been the center of attention for decades. Initially only appreciated by microbiologists for their utility in early forms of DNA sequencing and later as platforms for protein display in phage display technology,[1] they later garnered attention form colloid chemists in early 2000's for their ability to form chiral nematic liquid crystals, a self-organized structure that was out of reach for non-biological colloids,[2] and then by chemists for their ability to express peptides binding to non-organic ligands, such as metals and plastics.

Filamentous phages offer distinctive properties that present them as unique building blocks for the bottom up synthesis of advanced multifunctional material. Filamentous phage are semi-flexible proteinous nano-filaments with a very high aspect ratio (0.88 μm in length and 6.6 nm in diameter, with a molecular weight of 1.6×10^7 g/mol for wild type M13).[3] As one of the most widely investigated in this family, the M13 nanofilament is composed of 2700 copies of the major structural protein (protein 8) capped on each end with two different proteins. This protein shell encases a circular, single stranded DNA that encoded 11 genes, 5 of which code the 5 structural proteins of the virion. The remaining 6 genes are required to help the virus to infect its host bacterial cell and turn the bacterial cell into a factory for making thousands of M13 nano-filaments. The chemistry of the bacteriophage protein coat (all 5 structural proteins) can be controlled with atomic precision via genetic engineering, allowing for the expression of multiple different peptides/proteins/antibodies on the M13 protein coat, each offering specific interaction/recognition with a different ligand. This property alone makes the M13 nano-filaments superior to any and all synthetic nanoparticles. Combined with the ability of these nano-filaments to make thousands of identical copies of themselves under mild physiological conditions and at room temperature (simply by infecting a culture of host bacteria), and the ability to encode for new forms of specific recognitions via the powerful phage display technology, filamentous phage in general and M13 in particular claim a unique spot in a biological engineer's toolbox.

Previous reports on the use of phage M13 as a tool for material design demonstrate its utility in applications ranging from designing tissue engineering scaffolds to batteries.[4] Most of these efforts have focused less on the self-organization ability of M13 to form macrostructures, but more on the ability of M13 to be screened (through phage display) for peptides that bind to proteins, enzymes, cells, or minerals, hence providing a substrate with tunable specific recognition. The notable reports are the seminal paper by George Smith on creating a biosorbent mats with engineered M13 phage,[5] and the series of groundbreaking reports by Angela Belcher on using substrates coated with M13 displaying peptides that bind minerals or quantum dots used in energy storage devices.[6] The former, chemically crosslinked the M13 filaments to achieve a M13 mat and the latter, via chemical reactions,

physisorption, or electrostatic interactions, created films of M13 phage to be used a substrates/scaffolds for material design.[7]

In this work, we report on the inherent properties of self-organized, crosslinked M13 macrostructures that have not been identified previously. We demonstrate that M13 liquid crystals, crosslinked with a simple crosslinker such as glutaraldehyde exhibit advanced properties such autofluorescence that diminishes upon biodegradation and self-healing upon damage under physiological conditions. In addition, the M13 nanofilaments remain biologically active and able to infect their host bacterial cells in the crosslinked state. Our investigation focuses on M13 hydrogels composed of only two components, namely M13 and glutaraldehyde, and hence the properties observed are not a result of the functionality added by additional components or responsive crosslinkers.

3. Experimental Section

3.1. Bacteria and phage culture methods

Escherichia coli K12 ER2738 (New England Biolabs Ltd.), genotype: F´proA$^+$B$^+$ lacI^q Δ(lacZ)M15 zzf::Tn10(Tet^R)/ fhuA2 glnV Δ(lac-proAB) thi-1 Δ(hsdS-mcrB)5, was used as host for phage M13. Pre-cultures of host were prepared in LB-Miller broth (Fisher Scientific) using a single colony from fresh tetracycline plates (streaked from glycerol stocks) and incubated shaking at 37℃ overnight. The preculture was then diluted 1:100 in 250 mL of LB broth, to which 10 μL of M13 phage stock at 10^{12} plaque forming units (PFU) per mL was added. The phage culture was incubated shaking at 37℃ for 5 hours. The culture was subsequently centrifuged (7000×g, 15 min) to pellet bacteria. The supernatant, containing phage, was saved and stored at 4℃.

3.2. Phage purification and concentration

The crude phage stock purified via aqueous two-phase method, as described by Sambrook.[8] Briefly, a mixture of 20 (w/v)% PEG solution and 2.5M NaCl solution was added to the crude phage stock with a volumetric ratio of 1:6 and incubated at 4℃ overnight. Phage was pelleted by centrifugation (5000×g, 45 min, 4℃). The pellet was resuspended in 10 mL of RO Millipore water (resistivity=18.2 MΩ.cm) and incubated on a tube roller at 4℃ for 2 hrs. Tubes were subsequently centrifuged (5000×g, 15 min) to remove any residual bacterial

debris. This purification step was repeated twice and the resulting phage stock was then further purified and concentrated using Amicon Ultra centrifugal filters (Millipore Sigma, Ultra-15, MWCO 100 KDa and 30 KDa sequentially). The concentration of M13 phage was quantified using the plaque assay method, as described elsewhere.[9]

3.3. Preparation of phage hydrogels

Different concentrations of M13 phage suspension were prepared by making serial dilution of the purified, concentrated stock (10^{14} PFU/mL) in Millipore water. Next, in a 3 mL disposable syringe, phage was mixed with 1% or 2.5% glutaraldehyde and incubated at room temperature between 12 and 24 hrs. Inversion test was applied to verify the gelation. The hydrogels were then removed from the syringe and kept submerged in Millipore water at room temperature until used for subsequent experiments. Hydrogels were prepared fresh and used within a few hours for all experiments described below. Although they can be stable and stored in DI water at room temperature after producing.

3.4. Swelling test

Phage hydrogels were flash frozen with liquid nitrogen to decrease ice crystal formation and immediately freeze dried using Labconco lyophilizer. The dried gels were weighed and placed in 20 mL of 0.1 M pH=7.4 phosphate-buffered saline (PBS) at different temperatures (4, 25, and 37°C). The swollen gels were removed from the solution at the certain time intervals, after gently removing excess water with lint-free tissue paper, the gels were weighed using a Mettler analytical balance (readability 0.1 mg). Swelling ratio was calculated as follows by using the measure mass of wet gel (m_w) and dry gel (m_d): swelling ratio $(\%) = \frac{m_w - m_d}{m_d} \times 100$

3.5. Compression test and rheometry

Compression tests were carried out at 25°C using a Mach-1 Mechanical Tester (Biomomentum Inc, QC) with parallel-plate geometry. Prior to mechanical test, phage hydrogel discs were prepared with a diameter of 10 mm and a height of 2-4 mm. Compression testing was performed to 20% of the sample height at a rate of 0.03 mm/s. Preload force of 0.01 N and ramp force of 0.5 N/min were applied.

Rheological properties of runny phage hydrogel (6×10^{12} PFU/mL) were determined using an HR-2 Discovery Hybrid Rheometer (TA Instrument) equipped with Peltier plate Steel. A 1.005˚, 40 mm cone plate geometry with 100 μm truncation gap was used for all measurements. Dynamic rheological measurements were carried out at 25°C with a strain sweep between 0.1% and 100% and angular frequency was 10 rad/s.

3.6. Chemical characterization and spectrometry

UV-vis spectra of both the phage suspension and phage hydrogels in two different concentrations (3×10^{13} and 3×10^{14} PFU/mL) was recorded using a BioTek plate reader in the range of 200-900 nm. Wavelength scanning was performed between 200nm and 900 nm (whole range of UV-vis spectra) using a 96 well-plate. Attenuated total reflectance infrared (ATR-FTIR) spectra of phage solution and hydrogel were obtained with a Thermo Nicolet IR 560 system, using a Zn-Se ATR accessory (Thermo Electron Corporation, PA). Each sample was placed against the ATR element and the spectra were collected in the range of 500–4000 cm^{-1} using 128 scans at a resolution of 4 cm^{-1}. After acquisition, the IR spectra were baseline corrected for carbon dioxide peak at approximately 2750 cm^{-1}.

The fluorescence spectra for the phage suspension and the hydrogels was recorded using a Tecan fluorescence spectrometer. Phage hydrogel was prepared in a 3 mL cuvette. Excitation wavelength was set to vary from 370 nm to 600 nm with a 10 nm increments in each scan and emission wavelength was set from a wavelength slightly above the excitation wavelength to 800 nm.

3.7. Microscopy

The M13 suspension was coated on a silicon wafer substrate using convective assembly, as described elsewhere.[10] The samples were imaged using a Bruker Atomic Force Microscope (AFM) in air under tapping mode using a commercial n+-silicone cantilever, 240 μm long and 35 μm wide, with a resonant frequency of 50-130 kHz and spring constant of 9.0 N/m. The scanning rate was 1.0 Hz, at 0° angle.

For electron microscopy, the samples were prepared using two different methods, namely freeze-drying and critical-point drying. For freeze-drying, hydrogels were flash frozen in liquid nitrogen, freeze dried, then freeze fractured. For critical point drying, the hydrated

hydrogels were dehydrated using an ethanol gradient and dried for 3.5 hrs using a Leica critical point dryer (EM CPD300).

The samples were stored in a desiccator and prior to electron microscopy, were coated with a 10 nm layer of gold. Imaging was performed using at 10 kV a field emission scanning electron microscope (TESCAN VP. SEM).

The hydrogels were imaged in hydrated state using a Zeiss inverted fluorescence microscope with three sets of filters, namely ex/em = 358/461nm, ex/em = 470/530 nm and ex/em = 595/630 nm. The Excitation filter was placed in front of the LED light to excite the hydrogel with the specific wavelength and the Emission filter was attached on the camera to record the emission image of the phage hydrogel.

For polarized microscopy, an enclose chamber was created using a cleaned and dried glass slide and a cover slip. The coverslip was placed onto the glass slide, secured with parafilm on both sides and heated to 90℃ and removed when the parafilm became transparent. The M13 sample (or Milli-Q water for negative control) was pipetted into the confined chamber, which was then sealed with Vacuum Grease or nail polish, and incubated at 4℃. A saturated NaCl solution (36 (w/v) %) was placed in the petri dish to maintain 75% relative humidity. Samples were examined the following day using a Nikon light microscope equipped with polarizers, which were rotated at different angles using the 10× objective. Images were captured and analyzed using Motic imaging software.

3.8. Self-healing

For self-healing experiments, fully hydrated hydrogels were cut into two halves, the halves (from the same or different hydrogels) were put in a same shape mold and kept in contact in the presence of 2.6 mM calcium chloride and 0.5 and 0.25 (w/v) % solution of bovine serum albumin (BSA) at room temperature for 24-48 hrs. The healed hydrogel was taken out of the mold and used for either compression test or electron microscopy. Repeated self-healing was performed by cutting a healed hydrogel at a different location and repeating the procedure as described above.

4. Results and Discussion

4.1. Characterization of M13 hydrogels

The purified and concentrated phage stock, prepared using the method outlined in **Figure 2.1a**, was quantified to have 6×10^{14} PFU/mL. This stock was either used as full strength, or diluted in Millipore water to the desired concentration. A monolayer of M13 phage, assembled on silicon wafer can be seen in **Figure 2.1b**. Each phage filament is 6-8 nm thick and 850 nm. Therefore, the filaments visible in Figure 1b are bundles of phage and not a single filament.

Self-organization was induced in M13 suspensions with concentrations higher than 10^{14} PFU/mL via confinement at low temperature. The polarized light micrograph of the aligned M13 is presented in **Figure 2.1d**, compared to the micrograph recorded without cross-polarizers (**Figure 2.1e**). M13 has been reported to self-organize into lyotropic liquid crystals at 14-22 $mg/_{mL}$ (nematic phase) and 28-76 $mg/_{mL}$ (chiral nematic phase).[6] That is equivalent to 5×10^{14}-1×10^{15} phage particles per mL. Bacteria cell conditions and their even distribution over the plate is important to get an accurate result for plaque assay. Cells should be healthy, > 95% viable, and in log-phase growth at the time of the assay. Therefore, M13 quantification via plaque assay is known to underestimate the actual particle count by up to $10\times$, which means that the concentration used in this investigation is within the previously reported range for self-organization.

SEM images of the hydrogels (crosslinked with 1(w/v) % glutaraldehyde, critical-point dried) confirm a highly ordered structure. **Figure 2.2a** shows long-range order to the hydrogel layers. At higher magnification, a porous structure was observed **(Figure 2.2b)** composed of filaments, the size of which suggests M13 filament bundles of several hundred phages **(Figure 2.2c)**. Decreasing the phage concentration 10-fold (to 3×10^{13} PFU/mL) appears to decrease the long-range order of the hydrogel microstructure (**Figure 2.2d**), however a level of order still prevailed at higher magnification and filaments with a size suggestive of phage bundles of several hundred was visible (**Figure 2.2e**). For comparison, **Figure 2.2f**, shows the structure of a freeze-dried hydrogel, which, as expected, shows a different pore structure than critical-point dried hydrogels, likely as a results of ice crystal

formation. The ice crystals appear to have molded the phage bundles into thin sheets of M13, enveloping the larger pores, formed around the crystals.

(a)
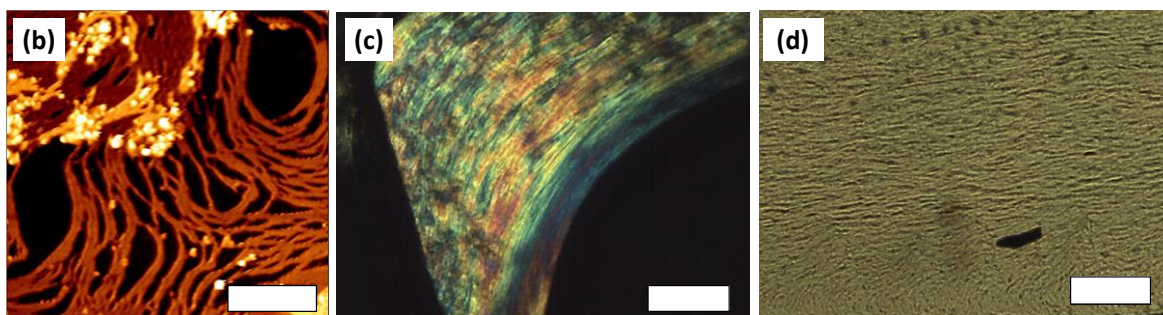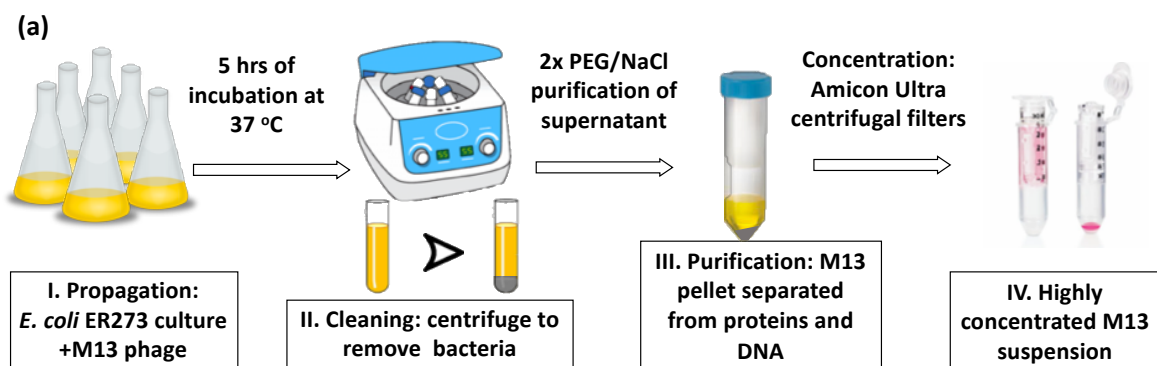
Figure 2.1- (a) Schematic representation of the process used to prepare high concentrations of pure M13 phage. The process starts by propagating M13 in an exponentially growing culture of host bacteria, which is then separated from phage via centrifugation. The crude phage stock was purified through two steps of PEG/NaCl precipitation followed by ultrafiltration. (b) AFM image of a monolayer of M13 phage assembled on freshly cleaved mica; the lighter portions are g3p's protruding from the end of the phage filaments. Scale bar represents 500 nm (c) The final concentrated M13 suspension, imaged with a polarized light microscope. Scale bar represents 100 μm. (d) the same phage suspension as part c, observed without polarizers. Scale bar in c and d represents 100 μm.
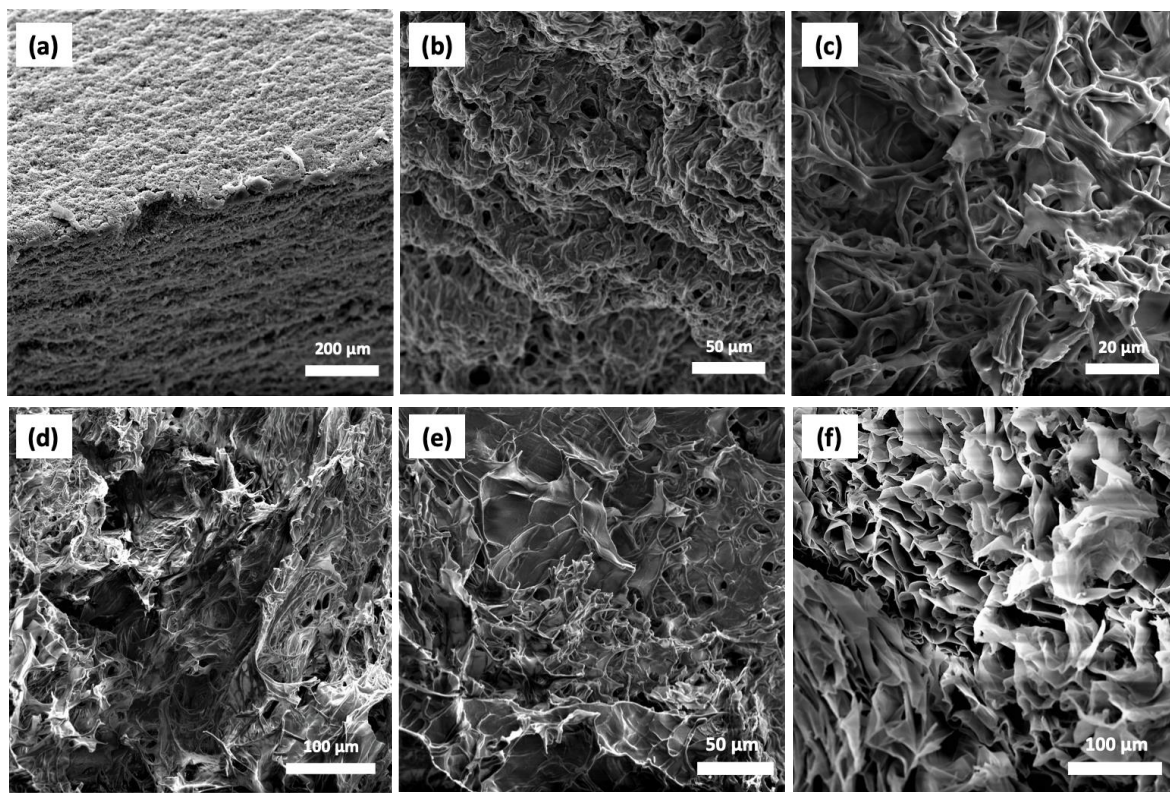
Figure 2.2- *Electron micrographs of M13 hydrogels prepared with a phage concentration of 3×10^{14} (**a,b,c**) and 3×10^{13} PFU/mL (**d,e,f**). All hydrogels were critical-point dried except for (**f**), which was freeze-dried.*

M13 phage formed hydrogels with concentrations as low as 6×10^{12} PFU/mL (**Figure 2.3a**). The test tube inversion method was used to confirm gelation. Depending on M13 phage titer, gelation time varies between 12 and 24 hrs. The gels formed with 6×10^{12} PFU/mL were very soft and did not hold their shape. They were proved to be crosslinked via rheometry. When compared to the viscosity of a viscous liquid (glycerol) and a phage suspension, the liquid-like hydrogel formed with 6×10^{12} PFU/mL of M13 showed a viscosity representative of crosslinked polymers and distinctly different from viscous liquids and the phage suspension as non-crosslinked liquid (**Figure 2.3b**). For all subsequent experiments, only hydrogels prepared with higher phage concentrations (higher than 6×10^{13} PFU/mL) were used. The stress-strain curve is presented in **Figure S2.1a**, which shows a typical trend for protein hydrogels, however, due to nonlinear curve, a global compression modulus of compression cannot be determined, therefore we calculated the slope of the stress-strain

curve at 0-5% strain. Moreover, the experimental observation showed that there was no breaking point of the hydrogels under pressure up to 25 N, although they were pressed with dimensional changes under this force. The M13 hydrogels exhibited a compression modulus of 5-9 KPa. Compression modulus increased slightly with increasing phage concentration; however, increasing the crosslinking density (using 2.5% glutaraldehyde rather than 1%) appeared to have a more marked effect on the compression strength of the hydrogels (**Figure 2.3c**). The crosslinking reaction occurs between ϵ -amino groups of lysine residues of the major capsid protein of M13 phage and two aldehyde groups in glutaraldehyde. During the process of gelation, glutaraldehyde, an aggressive carbonyl (–CHO) reagent, condenses amine groups of lysine residues on the phage coat protein, around 340 available lysine residues,[11] via Mannich reaction or reductive amination. Higher glutaraldehyde concentration suggests a higher crosslinking density, creating more junction points along each filament. This in turn can increase the stiffness of the hydrogel network, as demonstrated in **Figure 2.3c**.

The increase in network/crosslinking density, however, has an inverse effect on the M13 hydrogel swelling ratio. The hydrogel prepared with 3×10^{13} PFU/mL of M13 possesses the highest ratio of swelling of 15 times their dry weight (**Figure 2.3d**). The hydrogel prepared with 3×10^{14} PFU/mL of M13 only absorbed 11 times their dry weight in water. When the crosslinking density was increased (using 2.5% glutaraldehyde 3×10^{14} PFU/mL) the swelling ratio was only 700%. No temperature effect was observed for swelling (**Figure S2.1b**).
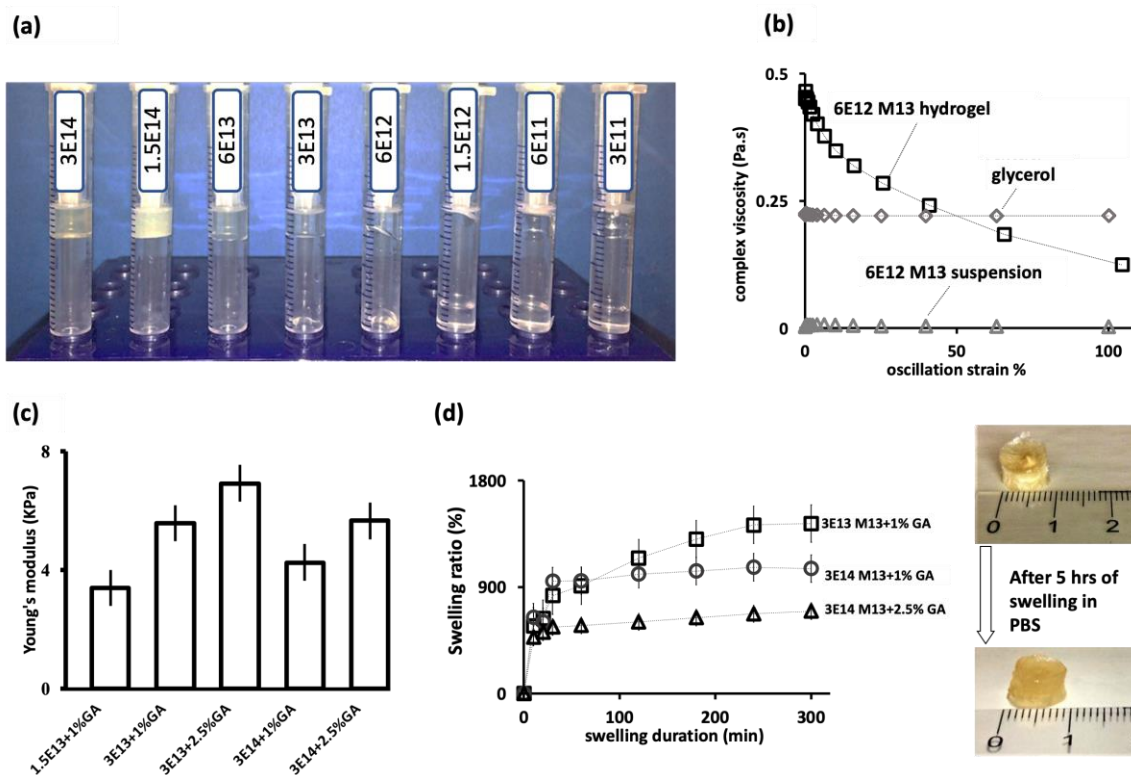
Figure 2.3- (a) Pictures of glutaraldehyde-crosslinked M13 gels made with different M13 concentrations. Concentrations are presented in terms of PFU/mL. All gels shown were crosslinked with 1% glutaraldehyde. (b) Rheology test for the lowest limit of M13 concentration to form a hydrogel compared to rheological behavior of a phage suspension with the same concentration and glycerol as reference. (c) Compression Modulus for M13 hydrogels shown in part b. (d) Swelling ratio for phage hydrogels with different M13 concentrations. Legend shows M13 concentration in PFU/mL+ Glutaraldehyde (GA) concentration in weight percent. Bottom; image of a freeze-dried M13 hydrogel before and after 5 hours of swelling in PBS.

4.2. Autofluorescence of M13 hydrogels

During the gelation process, a change in color was observed where the colorless, clear phage M13 suspension turned to a hydrogel with a yellow hue, which can be due to cyclic hemiacetal formations with glutaraldehyde, more visible at higher M13 concentrations. A UV-vis spectrum showed that M13 phage suspension has a sharp absorption peak at λ=280 nm, a typical absorption peak for proteins (**Figure 2.4a**). UV-Vis spectrum scanning from 200 nm to 500 nm for the M13 phage hydrogel demonstrated a new, relatively broad peak around

310 nm. To further investigation chemical change in the hydrogel, FTIR spectra of the hydrogel was analysed in comparison to the M13 suspension. Both the phage suspension and the hydrogel showed the same amide I peaks at ~1660 cm^{-1}, demonstrating amide bond in protein capsid of M13 phage (**Figure 2.4b**). In addition, the hydrogel exhibited amide II (~1570 cm^{-1}) and amide III bonds (~1280 cm^{-1}), marked on **Figure 2.4b**). There are multiple new absorption peaks (aside from those shared with glutaraldehyde and M13 suspension) that suggest new functional groups/new compounds formed.

During the crosslinking reaction, α,β-unsaturated aldehyde polymer can be formed, which leads to the C=C double bond existed in the system, accompanied by the C=N double bonds from Schiff's base.[12] The reaction between glutaraldehyde and amine groups may lead to side products, including Schiff's base with C=N bond, α,β-unsaturated (conjugated) Schiff's base with C=C bond, Michael addition product formed from α,β-unsaturated products, and dihyropyridine or dihydropyridinium which follow the ring closure of an intermediate during the reaction. [12]FT-IR peaks on **Figure 2.4b** shows a peak around 1480 cm^{-1} corresponding to imine (C=N) bond, and peaks between 1000 and 1200 cm^{-1} indicating C-N bond formed with Michael addition.

Further spectrometry revealed the M13 hydrogels to exhibit autofluorescence when excited at specific wavelengths. Emission spectra of M13 hydrogels and M13 suspensions were monitored with a fluorometer and the results show distinct peaks when excited at λ = 470 nm (**Figure 2.4c**), and λ = 598 nm (**Figure S2.2a**). As shown in **Figure 2.4c**, the spectra for glutaraldehyde, water, and M13 phage suspension do not show any similar peak on the same wavelengths.

Autofluorescence was confirmed using microscopy with three different optical filter sets (ex/em = 358/461 nm, ex/em = 498/509 nm, ex/em = 598/615 nm) and the hydrogels show blue, green and red autofluorescence (**Figure 2.4d** for 3×10^{14} PFU/mL, **Figure S2.2b** for 3×10^{13} PFU/mL,). Neither M13 phage suspensions (**Figure S2c, d**) nor glutaraldehyde (**Figure S2.2e**) show any autofluorescence when imaged with the same set of filters. Therefore, both spectrometry and microscopy suggest the existence of fluorescent molecule/functional group produced by M13 crosslinking with glutaraldehyde. However, this functional group could not be resolved via FTIR. Th origin of fluorescence remains to

be investigated; however, the fluorescence observed in the M13 hydrogel may be attributed, at least in part, to the electronic transitions such as π-π* transition of C=C bond and n-π* transition of C=N bond.[13]

Furthermore, when the M13 phage hydrogels were degraded using a 1 mg/mL solution of proteinase K (**Figure 2.4e**), the degradation products also exhibited autofluorescence (**Figure 2.4f**). Proteinase K has the ability to hydrolyze the amine bonds and break the ester bonds process in order to track the color changes. As shown in **Figure 2.4e**, the M13 phage hydrogel was mostly digested after 36 hrs at 37ºC. The color of the solution changed to yellow over time, consistent with the color of the hydrogel, which suggests the release of the fluorescent molecules produced in the crosslinking process. A hypothesis which was conformed via fluorescence microscopy. It is noteworthy that the red autofluorescence (ex/em 598/618) was no longer observed for the degradation product, providing a potential method to track biodegradation remotely for scenarios where the hydrogel is injected in tissue.
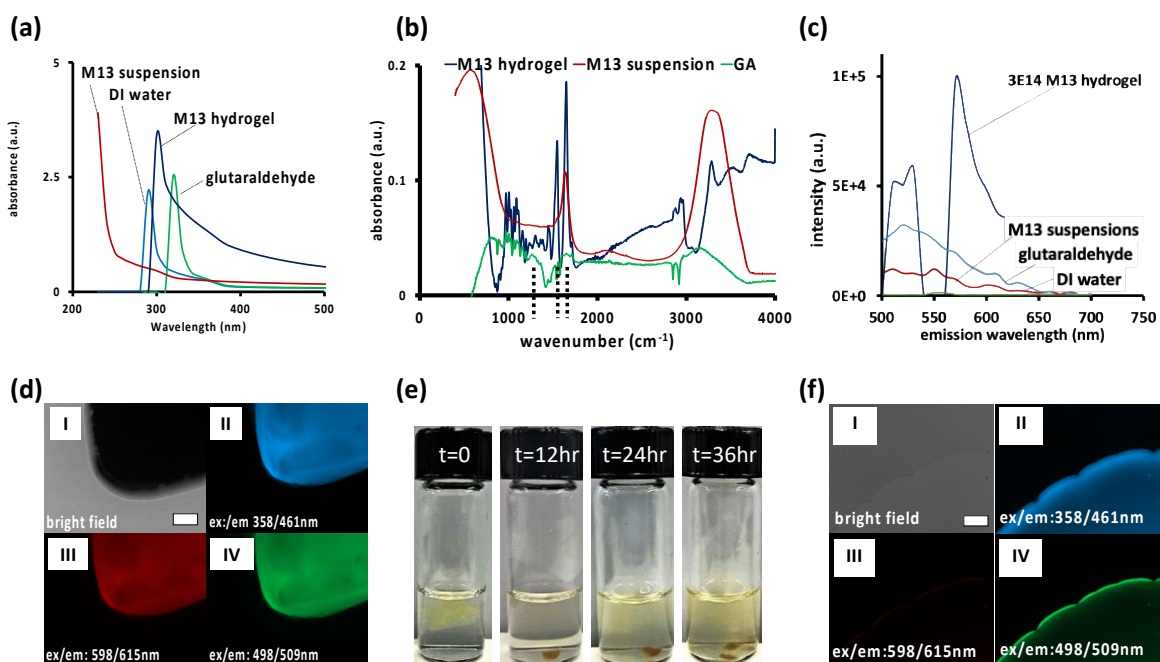
Figure 2.4- *(**a**) UV-Vis spectra of M13 suspension and M13 hydrogel. (**b**) The FTIR spectra for M13 hydrogel, M13 suspension and glutaraldehyde. The peaks for amide I, II, and III are marked with broken lines on x-axis. (**c**) Emission scan for M13 hydrogels when excited*

*at λ=470 nm. Emission scans show distinctive emission peaks for M13 hydrogels, different from the constituting components (M13, and glutaraldehyde, and water). (**d**) Fluorescence micrographs for hydrogel made with 3×10^{13} PFU/mL of M13: I. brightfield, II. hydrogel excited at 358 nm and imaged using a λ = 461 nm optical filter, III. hydrogel excited at 498 nm and imaged using a λ = 509 nm optical filter, IV. hydrogel excited at 598 nm and imaged using a λ = 615 nm optical filter. (**e**) M13 hydrogel digested by proteinase K. Images show biodegradation with time up to 36 hours. (**h**) Fluorescence micrographs for proteinase K degradation product of M13 hydrogel showing autofluorescence of degradation products. The gain was kept constant for all three excitation/emission pairs. Scale bar (c, d) =200 µm.*

4.3. Self-healing and bioactivity of M13 hydrogels

The M13 hydrogels prepared with both ~10^{14} and ~10^{13} PFU/mL of M13 exhibited repetitive self-healing capability at room temperature (**Figure S2.3**). Furthermore, M13 phage hydrogels made with two different concentrations of M13 suspension were shown to fuse together when put in contact in the presence of Ca^{2+} and BSA (**Figure 2.5a**). When the hydrogels, cut with a razor blade were incubated at room temperature in the presence of 2.6 mM CaCl$_2$ (extracellular physiological levels) and low concentrations of BSA, the hydrogels started to show signs of healing within hours, completely fusing back together into an intact hydrogel in 24-48 hrs. The fused hydrogel showed a lower compression modulus than the intact hydrogels (~4.4 and ~6.1 compared to ~9 for an intact hydrogel made with 3×10^{13} PFU/mL of M13), suggesting a degree of compromised mechanical strength (**Figure 2.5b**). Electron microscopy of the fused gel showed a scar than ran across the body of the gel, causing a disconnect in the order of the layers, but the layers were nonetheless fused together at the microscale (**Figure 2.5c,d**).

The M13 hydrogels that were incubated in the presence of Ca^{2+} but no BSA, showed no signs of healing after 48 hrs, whereas BSA concentrations as low as 0.125 (w/v)% induced self-healing, with a stress-strain response not significantly different form the hydrogels healed at higher BSA concentrations (**Figure 2.5b**). This observation suggests that residual aldehydes may be reacting with the amines in BSA or re-reacting with new lysines on M13. Since the crosslinking is probably due to Schiff's base in the first place, self-healing may be the reformation of Schiff's bases, most likely assisted by BSA/calcium interactions.

It could also be argued that BSA is important for the self-healing of M13 hydrogels. One might hypothesize that BSA is crosslinked in the presence of Ca^{2+}, thus healing the scar. However, for BSA to be physically crosslinked with Ca^{2+}, the protein must be first heated to thermally unfold the native BSA protein and form fibrillar BSA aggregates, then gelation is induced by adding fresh native BSA into the solution in the presence of Ca^{2+} at room temperature.[14] There are no reports of BSA being physically crosslinked with Ca^{2+} at room temperature without an initial step of heat-induced aggregation. The detailed mechanism for self-healing of M13 hydrogels as well as the role of BSA and the possible effect of other small proteins of M13 hydrogel self-healing remains to be investigated. In summary, the observation that our M13 hydrogels heal under physiological conditions in the presence of small proteins abundant in the body suggests that
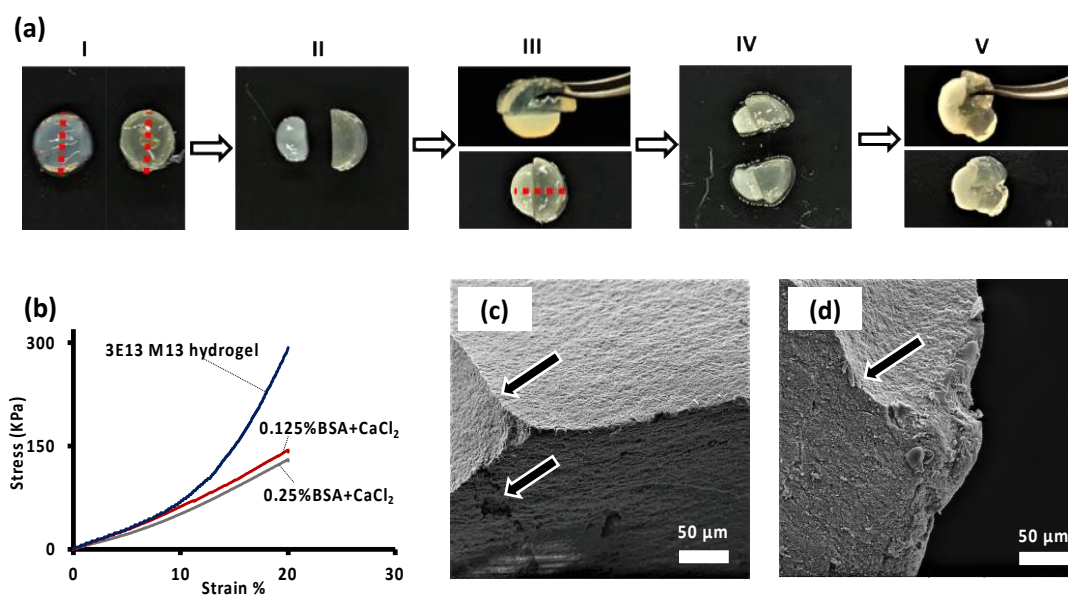
Figure 2.5- (a) *Phage hydrogels with two different M13 concentrations before and after repetitive healing in a 2.4 mM CaCl₂+0.5% BSA solution. I. M13 hydrogel made with 3×10¹³ PFU/mL (left) of phage and one with 3×10¹⁴ PFU/mL (right), II. Hydrogels in I, cut with a scalpel, III. Self-healed hydrogel after 48 hrs of incubation (top). Same self-healed hydrogel, marked by broken line on the location of new cut, IV. Same self-healed hydrogel, cut at a different location, V. self-healed after the second cut. Both scars are visible in the image. **(b)** compression behavior for M13 hydrogel before and after self-healing in different BSA concentrations. **(c,d)** SEM images of M13 hydrogel after self-healing, arrows show the location of the scar.*
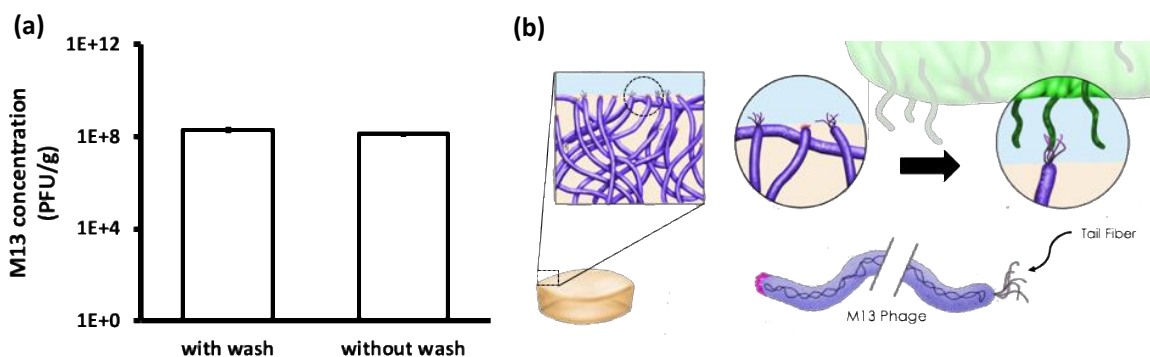
Figure 2.6- *(**a**) Bioactive property of M13 hydrogels demonstrated by the ability of M13 in the hydrogel to infect bacterial cells. The wash waters from the gels did not exhibit detectable levels of free M13. (**b**) Proposed mechanism for the observed bioactivity of the M13 phage hydrogels towards a culture of the host bacteria. (bottom) Schematic representation of the M13 phage filament, showing genome and the tail fibers (g3p).*

these hydrogels can be expected to exhibit self-healing similar to biological tissue where the healing processes are autonomously triggered after the damage.

In addition to self-healing, we also confirmed the biological activity of the M13 phage hydrogels by probing the ability of the constituting phage fibers to infect their bacterial host. We incubated the hydrogels with *E. coli* ER2738 (5hrs, 37℃), the culture showed a relatively high titer of phage suggesting the M13 phage inside the hydrogel, even though fixed in a matrix and chemically crosslinked, was still biologically active and able to infect its host bacteria and propagate itself (**Figure 2.6a**). To rule out the possibility of M13 leaking out of the hydrogels, we compared the results for freshly prepared hydrogels with hydrogels that were washed in Millipore water (10 water changes, 25 mL each). The washed hydrogel resulted in the same level of propagated phage as the non-washed hydrogel, when incubated with host bacteria (**Figure 2.6a**). This result also indicates that the any possible residues of the glutaraldehyde crosslinker used to prepare the hydrogel, was below toxicity levels to bacteria, because the bacteria were physiologically active to propagate the phage. We further checked the phage count in the wash waters used to wash the hydrogels. The concentration of M13 phage in the wash waters was below detection limit of the standard plaque assay, indicating minimal leaking out of M13 phage out of the hydrogels. This evidence further

confirms that m13 propagation in the presence of hydrogels in not a result of leaking of free M13 phage, but mainly a result of the preserved biological activity of M13 in our hydrogels. For M13 phage to infect its host bacteria, the phage uses a protein known as g3p (protein encoded by gene 3), a ~50 KDa protein situated protruding from the tip of the M13 phage filament with a copy number of 5 (**Figure 2.6b**). In fact, the lighter spots (higher elevation) in the AFM image in **Figure 2.1b** are the protruding g3p's. We propose that the g3p's for some of the M13 filaments, crosslinked in the hydrogel network are exposed and available through the surface of the hydrogel and the surface of the pores to bind host bacteria (**Figure 2.6b**). Binding is known to initiate the insertion of the M13 genome into the bacterial cell and start the infection and M13 propagation cycle.[15] This means that even if M13 filaments are not available to freely diffuse through the environment and bind to their host cells (as they do in the typical phage propagation cycle, they can still infect host bacteria, thus maintaining their cherished biological activity in the hydrogel. This is welcome news, because g3P is the protein most widely used for phage display, a screening technology aimed at uncovering peptides that show high specificity for organic and inorganic substrates of interest,[16] allowing for the development of M13 hydrogels that show specific affinity towards targets as diverse as environmental contaminants to cancer cell biomarkers. The bioactivity of the M13 hydrogels is, however, not limited to g3p; protein 8 (coating the entire length of the fiber, minus the two ends) is also widely used for expressing recombinant peptides. This protein has a significantly higher copy number of 2500-2700 and coats the entire phage filament (except for the tips), thus offering more binding sites for binding of desired ligands in a M13 hydrogel made with genetically engineered M13 filaments, further expanding the applications and impact of these hydrogels as a multifunctional material.

5. Conclusion

We introduce a novel functional material composed solely of self-organized M13 filamentous phage (crosslinked with glutaraldehyde, a non-responsive crosslinker) and demonstrate three major properties for these hydrogels, namely autofluorescence, self-healing, and bioactivity. Previous reports of crosslinked structures made with M13 phage do not report any advanced functionality other than biorecognition of specific ligands, a

property designed into the genome of the genetically engineered phage. Combining the crosslinked phage with responsive crosslinkers, or plasmonic nanoparticles,[17] however, resulted in macrostructures that exhibited the advanced properties of the crosslinkers (*e.g.*, pH responsiveness[18]) or the nanoparticle along with the biological recognition ability of the genetically engineered phage. Our investigation highlights the utility of M13 bacteriophage as a powerful building block in its own right for bottom-up assembly of multifunctional bioactive material with advanced functionalities such as fluorescence and self-healing. Paired with the ability of the M13 nano-biofilament to self-replicate and to be readily lend itself to genetic engineering, M13 and its self-organized macrostructures are a powerful new class of advanced multifunctional bioactive material. It is noteworthy that, as attractive as these properties are, to make the most of the powerful properties of the M13 nano-biofilament, calls for more mechanistic investigations into the different properties reported in this investigation.

6. Supplementary Information
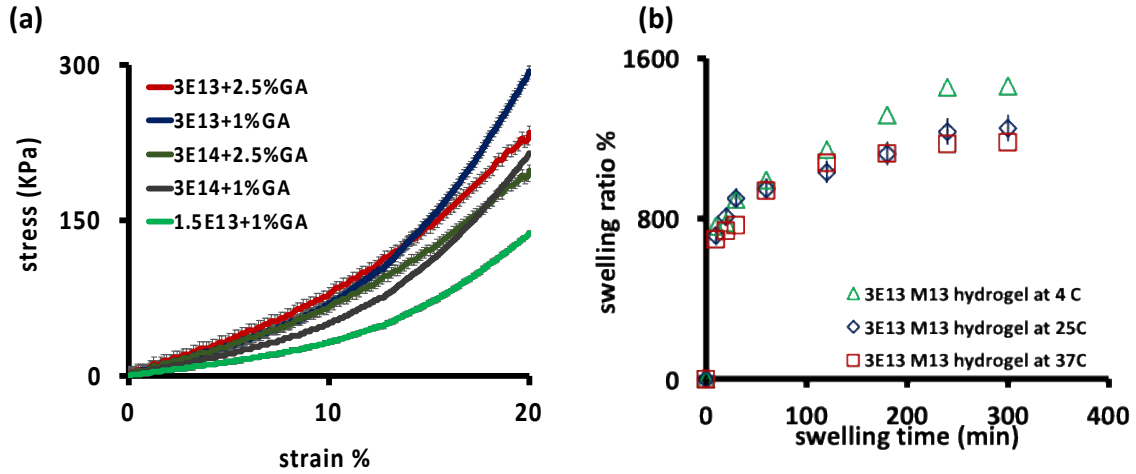
Figure S2.7- ***(a)*** *stress-strain curve for M13 phage hydrogels.* ***(b)*** *Swelling ratio for 3×10^{13} PFU/mL hydrogels at different temperatures.*
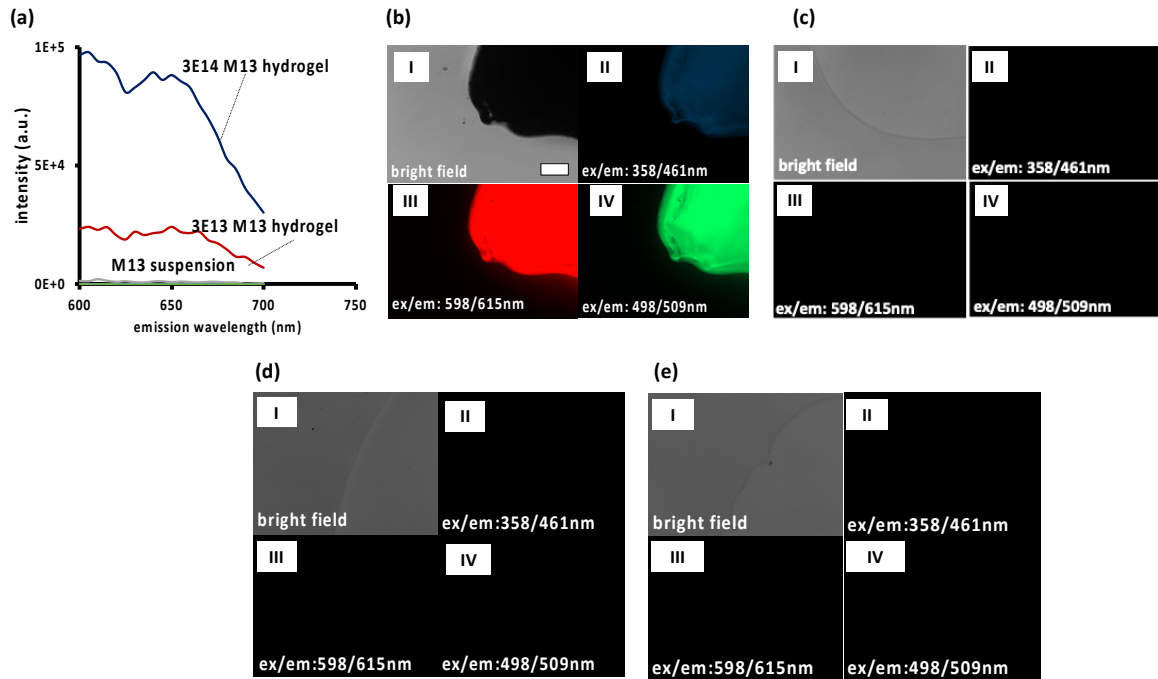
Figure S2.8- ***(a)*** *Emission scans when excited at λ =598 nm, respectively. Fluorescence images of* ***(b)*** *3×10^{14} PFU/mL M13 phage hydrogel,* ***(c)*** *3×10^{14} PFU/mL M13 phage suspension,* ***(d)*** *3×10^{13} PFU/mL M13 phage suspension,* ***(e)*** *glutaraldehyde. Scale bar (b-e)=200 µm.*
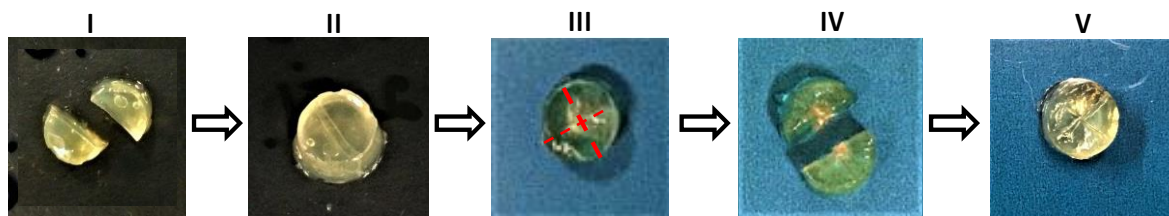
Figure S2.9- *Phage hydrogel before and after repetitive healing in a 2.4 mM CaCl$_2$+0.5% BSA solution. I. M13 hydrogel made with 3×10^{13} PFU/mL of phage, cut II. Hydrogels in I, self-healed hydrogel after 48 hrs of incubation. III. Same self-healed hydrogel, marked by broken lines on the location of the old and new cut, IV. Hydrogel in III, cut, V. self-healed hydrogel, after the second cut. Both scars are visible in the image.*

7. References

1   Smith, G. P. Filamentous fusion phage: Novel expression vectors that display cloned antigens on the virion surface. *Science* **228**, 1315-1317, (1985).

2   Cao, J., Liu, S., Xiong, J., Chen, Y. & Zhang, Z. Stimuli responsive chiral liquid crystal phases of phenylboronic acid functionalized rodlike viruses and their interaction with biologically important diols. *Chem. Commun.* **50**, 10402-10405, (2014).

3   Dogic, Z. & Fraden, S. Ordered phases of filamentous viruses. *Current Opinion in Colloid & Interface Science* **11**, 47-55, (2006).

4   Lee, J. H. *et al.* Production of tunable nanomaterials using hierarchically assembled bacteriophages. *Nat. Protocols* **12**, 1999-2013, (2017).

5   Smith, G. P., Petrenko, V. A. & Matthews, L. J. Cross-linked filamentous phage as an affinity matrix. *J. Immunol. Methods* **215**, 151-161, (1998).

6   Lee, S.-W., Mao, C., Flynn, C. E. & Belcher, A. M. Ordering of Quantum Dots Using Genetically Engineered Viruses. *Science* **296**, 892-895, (2002).

7   Chiang, C.-Y. *et al.* Weaving Genetically Engineered Functionality into Mechanically Robust Virus Fibers. *Adv. Mater.* **19**, 826-832, (2007).

8   Sambrook, J. & Russell, D. W. *Molecular cloning: a laboratory manual*. 3 edn, (Cold Spring Harbour laboratory Press, 2001).

9   Kropinski, A. M., Mazzocco, A., Waddell, T. E., Lingohr, E. & Johnson, R. P. in *Bacteriophages: Methods and Protocols, Volume 1: Isolation, Characterization, and Interactions*   (eds Martha R. J. Clokie & Andrew M. Kropinski) 69-76 (Humana Press, 2009).

10   Malaquin, L., Kraus, T., Schmid, H., Delamarche, E. & Wolf, H. Controlled Particle Placement through Convective and Capillary Assembly. *Langmuir* **23**, 11513-11521, (2007).

11   Chung, W.-J., Lee, D.-Y. & Yoo, S. Y. Chemical modulation of M13 bacteriophage and its functional opportunities for nanomedicine. *International Journal of Nanomedicine* **9**, 5825-5836, (2014).

12   Cheung, D. T. & Nimni, M. E. Mechanism of crosslinking of proteins by glutaraldehyde I: reaction with model compounds. *Connect. Tissue Res.* **10**, 187-199, (1982).

13   Wei, W. *et al.* Preparation and Application of Novel Microspheres Possessing Autofluorescent Properties. *Adv. Funct. Mater.* **17**, 3153-3158, (2007).

14   Chen, J., Dong, Q., Ma, X., Fan, T.-H. & Lei, Y. Repetitive Biomimetic Self-healing of Ca^{2+}-Induced Nanocomposite Protein Hydrogels. *Sci. Rep.* **6**, 30804, (2016).

15   Calendar, R. L. *The Bacteriophages*. second edn, (Oxford University Press, 2006).

16   Smith, G. P. & Petrenko, V. A. Phage Display. *Chem. Rev.* **97**, 391-410, (1997).

17   Souza, G. R. *et al.* Networks of gold nanoparticles and bacteriophage as biological sensors and cell-targeting agents. *Proceedings of the National Academy of Sciences* **103**, 1215-1220, (2006).

18   Chen, L., Zhao, X., Lin, Y., Su, Z. & Wang, Q. Dual stimuli-responsive supramolecular hydrogel of bionanoparticles and hyaluronan. *Polymer Chemistry* **5**, 6754-6760, (2014).

Chapter 3 – Structure and Properties of Hybrid Phage-BSA Hydrogels

1. Abstract

Filamentous phages (bacterial viruses) have been extensively explored in their capacity as a bionanoparticle for applications ranging from design of tissue engineering scaffolds to energy storage devices. Filamentous phages are proteinous nanofilaments for which surface chemistry can be controlled with atomic precision via genetic engineering, a property that makes them superior to synthetic nanoparticles. We have previously reported M13 phage hydrogels formed with self-organized M13 phage with a range of advanced properties. These hydrogels, however, need a very high concentrations of M13, to achieve lyotropic liquid crystalline phase, requiring a laborious and lengthy concentration procedure that could limit their utility. Here, we report the formation of M13 hydrogels with lower concentrations of phage, up to 100×, through synergistic action with a very low concentration (0.25 w/v%) of the small globular protein, Bovine serum albumin. Neither component gels on its own at these low concentrations, indicating a shift in the phase diagram for M13, inducing self-organizations at lower concentrations. The hybrid hydrogels exhibit 2× higher ability to pack water compared to BSA only hydrogels and 5× higher compression compression modulus compared to M13 only hydrogels. In addition, the hybrid hydrogels exhibit self-healing under physiological conditions, autofluorescence, and biological activity towards host bacterial cells. Our report highlights the importance of further mechanistic investigations into the nature of the phase diagram for filamentous phage in the presence of different proteins of biological relevance, which might open avenues for the development of stimulus-responsive biomaterials with M13 phage.

2. Introduction

Natural polymers have long garnered interest as building blocks for biomaterials. Natural polymers such as cellulose,[1] starch,[2] collagen,[3] silk,[4] and chitosan[5] have been reported to

form hydrogels via physical or chemical crosslinking. Natural polymers are biodegradable and biocompatible by nature and they do not release toxic materials upon degradation. As a special class of natural polymers, proteins and peptides offer several functional groups that make them amenable to a range of chemical reactions, allowing for chemical crosslinking, loading of different drugs, and chemistries enabling trigger-responsive release.[6] One of the drawbacks of proteins and peptides for making hydrogels is the possibility of denaturation in the gelation process and the limited bioactivity offered by the protein. For biomaterials in general, and hydrogels in particular, specific interaction and biorecognition of select ligands (chemicals, contaminants, disease biomarkers) is a highly desired property. However, each protein/peptide offers only a single biorecognition ability, limiting the utility of protein/peptide hydrogels as multifunctional bioactive materials. This limitation can be overcome using another class of natural compounds, namely viral nanoparticles, specifically bacteriophages.

Bacteriophages, or phage for short, are viruses that infect bacteria. Phages offer remarkable diversity in terms of both genomic sequence and physical appearance and can be found in many shapes and sizes.[7] Phages are essentially proteinous nanoparticles that are amenable to all chemistries applicable to proteins, with the additional characteristic that the chemistry of the bacteriophage protein coat can be controlled with atomic precision via genetic engineering, a property that makes them superior to synthetic nanoparticles.

Filamentous phages of *Escherichia coli* (*f1*, *fd* and M13) are proteinouse nanofilaments a high aspect ratio and circular DNA genome.[8] Filamentous phage offer properties that present them as unique building blocks for the bottom up synthesis of advanced material. Phage M13, in particular, has been extensively explored in its capacity as a bionanoparticle for applications ranging from design of tissue engineering scaffolds to batteries.[9] Wild-type M13 is 0.88 μm long and has a diameter D=6.6 nm, and molecular weight M=1.6×10^7 g/mol.[10] M13 filaments self-organize into lyotropic or concentration-induced liquid crystals at high concentrations (>14 $mg/_{mL}$).[11] Furthermore, these ordered structures have been used to form highly ordered films that are then utilized as scaffolds for mineralizing metals or other elements[12] or for making biosensing surfaces.[13,14] In a

previous manuscript, we reported M13 hydrogels formed with self-organized M13 phage with a range of advanced properties. These hydrogels, however, require very high concentrations of M13 requiring a laborious and lengthy concentration procedure that could limit their utility.

In this work we report the formation of M13 hydrogels at lower concentrations simply by adding a very low concentration of the small globular protein, BSA (bovine serum albumin) at concentrations so low that BSA would not gel alone. Neither would M13 phage at the low concentrations used, indicating synergistic action between M13 phage and BSA. We hypothesize that BSA shifts the phase diagram for M13, inducing self-organizations at lower concentrations much lower than $14 \, ^{mg}/_{mL}$, the reported onset of formation of sematic phase. Addition of spherical micro/nano particles[15] and non-adsorbing proteins[10] have been shown to shift the phase diagram for rod like particles or filamentous phage suspensions. We further investigate the swelling and mechanical properties of these hybrid hydrogels and demonstrate that similar to pure M13 hydrogels, they exhibit self-healing, autofluorescence, and biological activity towards host bacterial cells.

1. Experimental Section

   1.1. Bacteria and phage culture methods

Escherichia coli K12 ER2738 (New England Biolabs Ltd.), genotype: F´proA⁺B⁺ lacIq Δ(lacZ)M15 zzf::Tn10(TetR)/ fhuA2 glnV Δ(lac-proAB) thi-1 Δ(hsdS-mcrB)5, was used as host for phage M13. Pre-cultures of host were prepared in LB-Miller broth (Fisher Scientific) using a single colony from fresh tetracycline plates (streaked from glycerol stocks) and incubated shaking at 37℃ overnight. The preculture was then diluted 1:100 in 250 mL of LB broth, to which 10 μL of M13 phage stock at 10^{12} plaque forming units (PFU) per mL was added. The phage culture was incubated shaking at 37℃ for 5 hours. The culture was subsequently centrifuged (7000×g, 15 min) to pellet bacteria. The supernatant, containing phage, was saved and stored at 4℃.

1.2. Phage purification and concentration

The crude phage stock purified via aqueous two-phase method, as described by Sambrook.[16] Briefly, a mixture of 20 (w/v)% PEG solution and 2.5M NaCl solution was added to the crude phage stock with a volumetric ratio of 1:6 and incubated at 4℃ overnight. Phage was pelleted by centrifugation (5000×g, 45 min, 4℃). The pellet was resuspended in 10 mL of RO Millipore water (resistivity=18.2 MΩ.cm) and incubated on a tube roller at 4℃ for 2 hrs. Tubes were subsequently centrifuged (5000×g, 15 min) to remove any residual bacterial debris. This purification step was repeated twice. The concentration of M13 phage was quantified using the plaque assay method, as described elsewhere.[17]

1.3. Preparation of hydrogels

Different concentrations of M13 phage suspension and BSA solution were prepared by making serial dilution of the purified, concentrated stock in Millipore water. Next, in a 3 mL disposable syringe, M13 phage was mixed with BSA and glutaraldehyde and incubated at room temperature for a few minutes to 24 hrs. Inversion test was applied to verify the gelation. Gelation time was recorded as the time when the crosslinked protein/M13 stops flowing out of inverted tubes and recorded at 25℃. The hydrogels were then removed from the syringe and kept submerged in Millipore water at room temperature until used for subsequent experiments. Hydrogels were prepared fresh and used within a few hours for all experiments described below.

1.4. Swelling test

Phage hydrogels were flash frozen with liquid nitrogen to decrease ice crystal formation and immediately freeze dried using Labconco lyophilizer. The dried gels were weighed and placed in 20 mL of 0.1 M pH=7.4 phosphate-buffered saline (PBS) at different temperature (4, 25, and 37℃). The swollen gels were removed from the solution at the certain time intervals, after gently removing excess water with lint-free tissue paper, the gels were weighed using a Mettler analytical balance (readability 0.1 mg). Swelling ratio was calculated as follows by using the measure mass of wet gel (m_w) and dry gel (m_d): swelling ratio (%) $= \frac{m_w - m_d}{m_d} \times 100$

1.5. Compression test

Compression tests were carried out at 25℃ using a Mach-1 Mechanical Tester (Biomomentum Inc, QC) with parallel-plate geometry. Prior to mechanical test, phage hydrogel discs were prepared with a diameter of 10 mm and a height of 2-4 mm. Compression testing was performed to 20% of the sample height at a rate of 0.03 mm/s. Preload force of 0.01 N and ramp force of 0.5 N/min were applied.

1.6. Chemical characterization and spectrometry

UV-vis spectra of both the phage suspension, hybrid phage hydrogels and BSA solution was recorded using was recorded using a BioTek plate reader in the range of 200-900 nm. Wavelength scanning was performed between 200nm and 900 nm (whole range of UV-vis spectra) using a 96 well-plate. Attenuated total reflectance infrared (ATR-FTIR) spectra of phage solution and hydrogel were obtained with a Thermo Nicolet IR 560 system, using a Zn-Se ATR accessory (Thermo Electron Corporation, PA). Each sample was placed against the ATR element and the spectra were collected in the range of 500–4000 cm^{-1} using 128 scans at a resolution of 4 cm^{-1}. After acquisition, the IR spectra were baseline corrected for carbon dioxide peak at approximately 2750 cm^{-1}.

1.7. Microscopy

For electron microscopy, the samples were prepared using two different methods, namely freeze-drying and critical point drying. For freeze-drying, hydrogels were flash frozen in liquid nitrogen, freeze dried, then freeze fractured. For critical point drying, the hydrated hydrogels were dehydrated using an ethanol gradient and dried using a Leica critical point dryer (EM CPD300). The samples were stored in a desiccator and prior to electron microscopy, were coated with a 10 nm layer of gold. Imaging was performed using at 10 kV a field emission scanning electron microscope (TESCAN VP. SEM).

The hydrogels were imaged in hydrated state using a Zeiss inverted fluorescence microscope with three sets of filters, namely ex/em = 358/461nm, ex/em = 470/530 nm and ex/em = 595/630 nm. The Excitation filter was placed in front of the LED light to excite the hydrogel with the specific wavelength and the Emission filter was attached on the camera to record the emission image of the phage hydrogel.

1.8. Self-healing

For self-healing experiments, fully hydrated hydrogels were cut into two halves, the halves (from the same or different hydrogels)were put in a same shape mold and kept in contact in the presence of 2.6 mM calcium chloride at room temperature for 24 hrs. The healed hydrogel was taken out of the mold and used for either compression test or electron microscopy. Repeated self-healing was performed by cutting a heled hydrogel at a different location and repeating the procedure as described above.

2. Results and Discussion

2.1. Physical and chemical characterization of hybrid M13 hydrogels

M13 phage at 2×10^{12} PFU/mL, prepare using the method depicted in **Figure 1a**, was crosslinked with different BSA concentrations using glutaraldehyde as a crosslinker. The reaction occurs between amine groups in lysin residues of M13 phage (~340) and BSA (30-35) protein with two aldehyde groups in glutaraldehyde.[18] BSA concentrations as low as 0.25 w/v% resulted gelation, whereas lower BSA concentrations lead to a degree of transparency change in the mixture, but the mixture would flow freely, and M13 would not gel without any BSA (**Figure 1b**). it is noteworthy that BSA alone in DI water does not gel at concentrations below 3 w/v% (**Figure 1c**). The fact that neither of the two components comprising the hybrid hydrogels are able to form a gel alone, suggests synergy between M13 and BSA in forming the hydrogel. We further measured gelation time using the test tube inversion method (**Figure S1a**). As expected, the gelation time increased exponentially with decreasing BSA concentration. During the process of gelation, glutaraldehyde, an aggressive carbonyl (–CHO) reagent, condenses amine groups of lysine residues on the phage coat protein as well as BSA protein via Mannich reaction or reductive amination. However, this reaction is known to be highly concentration dependent, activating the lysin residues on the same particle/molecule without any effective crosslinking at low concentrations. We conformed these reports by adding high concentration (~10^{14} PFU/mL) M13 to a 2-week-old M13 (2×10^{12} PFU/mL)-glutaraldehyde mixture (kept at room temperature), which did not gel during the two weeks at room temperature, after which immediate gelation was observed (data not shown). We hypothesized that BSA shifts the

phase diagram for M13, inducing self-organizations concentrations much lower than the onset of formation of sematic phase. This hypothesis remains to be investigated.

When comparing hydrogels of BSA alone (at 3w/v%, the limit of BSA solo gelation) and hybrid M13 -BSA hydrogels (same BSA concentration), hydrogels with M13 showed a significantly higher swelling ratio (~15× their dry weight) compared to hydrogels with BSA alone (~4× their dry weight). Decreasing BSA concentration from 3 to 1% slightly increased swelling ratio to ~15× their dry weight, suggesting a possible change in pore structure in the presence of BSA (**Figure 3.2a**). Swelling at temperatures other than room temperature (25℃) showed a marked decrease (swelling ratio decreased to half)with increasing swelling temperature to 37℃, but no effect at lower temperatures (**Figure 3.2b**). SEM images of the hybrid M13-BSA hydrogels (1% BSA, crosslinked with 1(w/v)% glutaraldehyde, critical point dried) reveal microporous structure (**Figure 3.3a,b).** For comparison, **Figure 3.3c,d** shows the structure of a freeze-dried hydrogel, which, as expected, shows a larger pore size than critical point dried hydrogels, likely as a results of ice crystal formation. Furthermore, comparing the pore structure of hybrid M13-BSA (3%) hydrogels (**Figure 3.3e,f**) with BSA hydrogels with the same concentration of BSA **(Figure 3.3g,h)** reveals the hybrid M13-BSA hydrogels to have a finer pore structure, with shapes that are distinctly different, partially explaining the difference observed in swelling ratio.
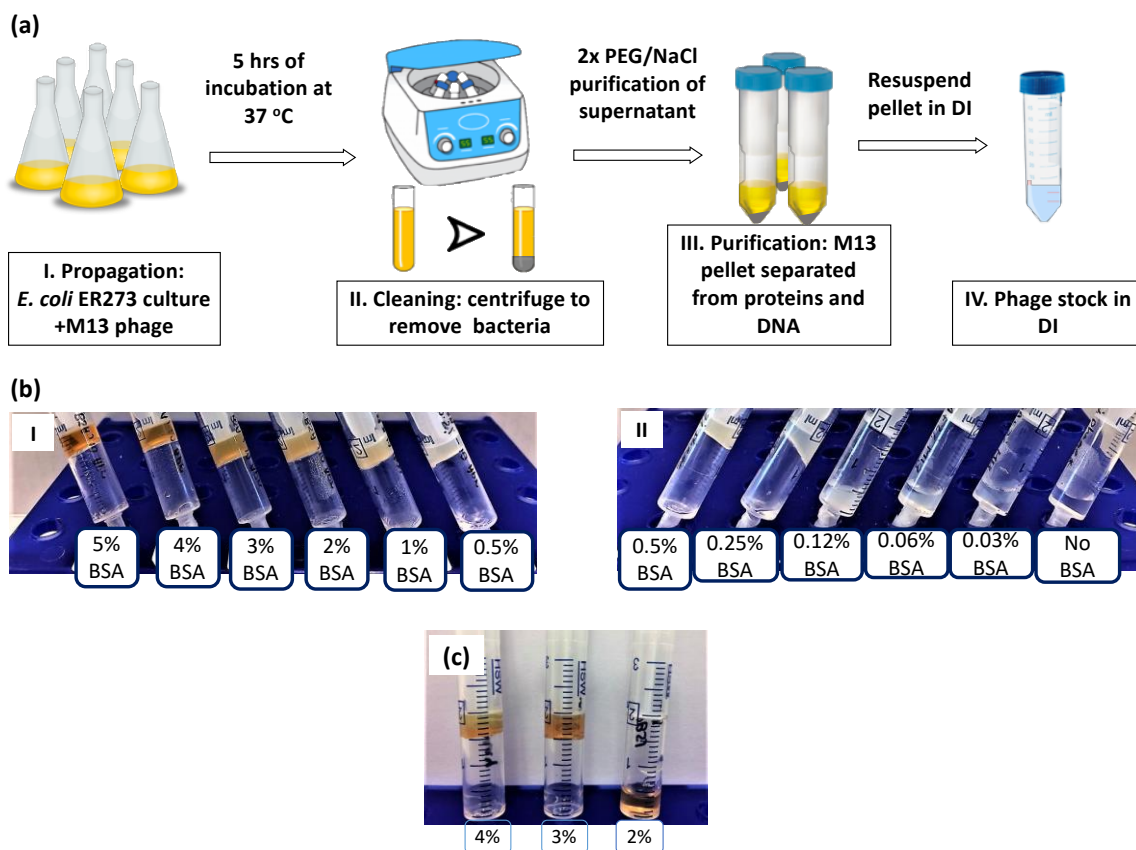
Figure 3.1- (*a*) *Schematic representation of the process used to prepare and purify M13 phage. The process starts by propagating M13 in an exponentially growing culture of host bacteria, which is then separated from phage via centrifugation. The crude phage stock was purified through two steps of PEG/NaCl precipitation and resuspended in DI water. (b) Images of hydrogels; I, II. pictures of glutaraldehyde-crosslinked hybrid M13-BSA hydrogels made with 2×10^{12} PFU/mL of M13 and different BSA concentrations. (c) Hydrogels of BSA only, crosslinked with glutaraldehyde. BSA concentrations are presented in w/v%.. All gels shown were crosslinked with 1% glutaraldehyde.*
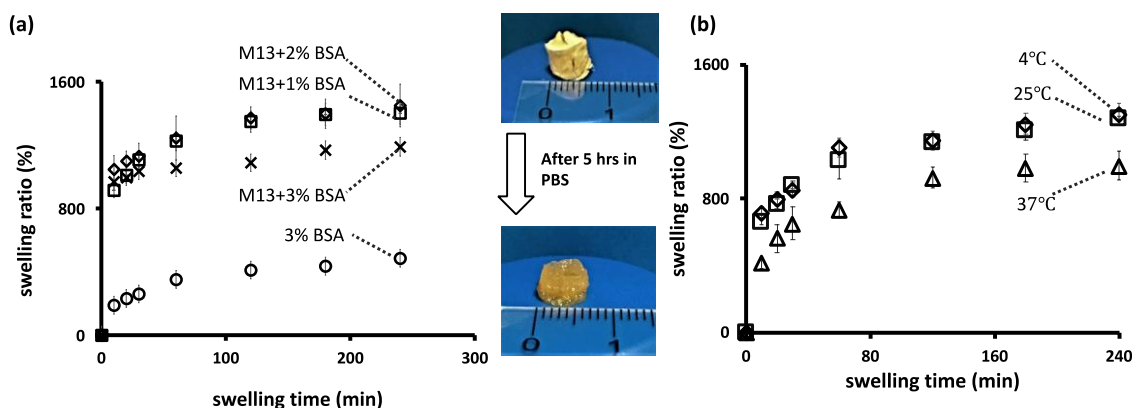
Figure 3.2- *(**a**) Swelling ratio for hybrid M13-BSA hydrogels with different concentration of BSA. Image shows picture of a freeze-dried hybrid M13-BSA(1%) hydrogel after 5 hours swelling at 25℃.* (***b***) *Effect of temperature on swelling ratio of the hybrid M13-BSA hydrogels.*

Addition of BSA, however, appeared to have strengthened the hydrogels, based on the stress-strain response curves in **Figure 3.4a**. The increase of BSA percentage from 1 to 3% significantly increased the amount of stress the hybrid hydrogels could sustain. The compression test results in a nonlinear curve, making the calculation of a global compression modulus of compression difficult, therefore we calculated the initial slope of the stress-strain curve. The experimental observation showed that there was no breaking point of the hydrogels under pressure up to 25 N, although they were pressed with dimensional changes under this force. The hybrid M13+1% BSA hydrogels exhibited a compression modulus of 0.2 KPa that increased to 1.6 KPa for M13+3% BSA hydrogels, a value similar to that for BSA only hydrogels. For applications that require soft hydrogels, M13 hydrogels are ideal, however should mechanical strength be desired, these hydrogels can be strengthened by adding natural nanoparticles known for their mechanical strengths, such as cellulose nanocrystals.
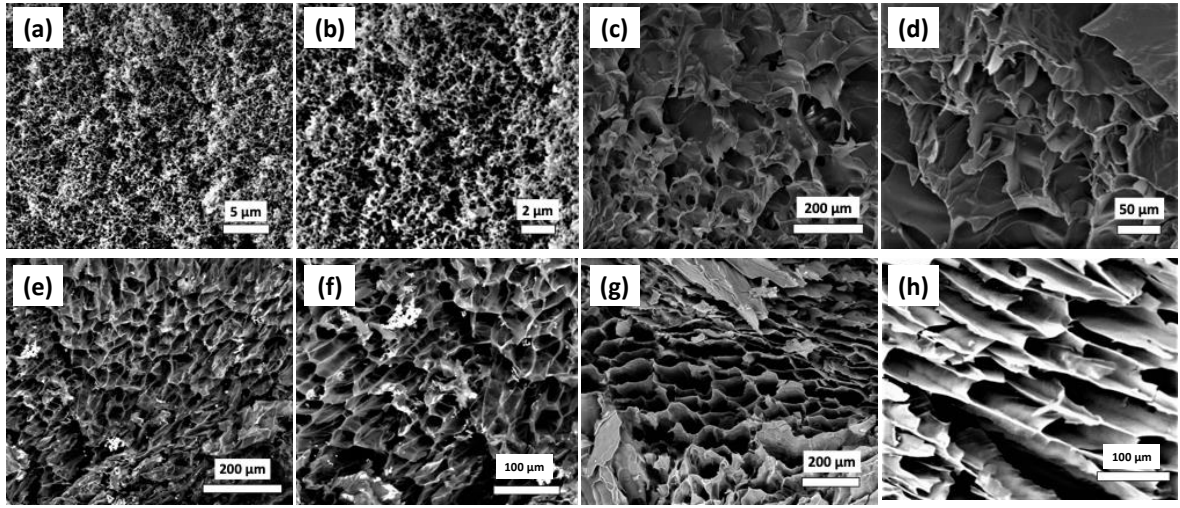
Figure 3.3- *Scanning electron micrographs of (**a,b**) hybrid M13+1% BSA hydrogel, critical point dried; (**c,d**) hybrid M13+1% BSA hydrogel, freeze dried; (**e,f**) hybrid M13+3% BSA hydrogel; (**g,h**) 3% BSA hydrogel.*
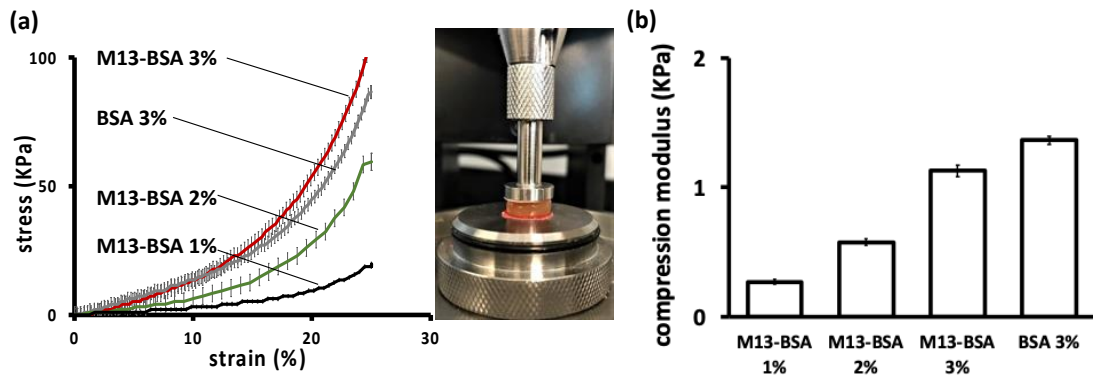
*Figure 3.4- (**a**) Stress-strain response for hybrid M13-BSA and BSA hydrogels; image shows a hybrid M13-BSA hydrogel under compression load. (**b**) Compression modulus for hybrid M13-BSA and BSA hydrogels.*

2.2. Autofluorescence of hybrid M13 hydrogels

The hybrid M13-BSA hydrogels and the BSA only hydrogels, both exhibited autofluorescence. However, while BSA only hydrogels showed autofluorescence at red and green wavelengths (**Figure 3.5b**), hybrid M13-BSA hydrogels auto fluoresced at green,

red, and blue wavelengths (**Figure 3.5a**). Autofluorescence with the optical filter set ex/em = 358/461 nm, appears to be an added property of M13 hydrogels, since it was also observed in our previous report with M13 only hydrogels. BSA solution (**Figure S1b**), M13 phage suspensions (**Figure S1c**), glutaraldehyde (**Figure S1d**) do not show any autofluorescence when imaged with the same set of filters. To investigate possible production of fluorescent chemicals, FTIR spectra of the hybrid hydrogel was analysed in comparison to the M13 suspension and glutaraldehyde. Both the phage suspension and the hydrogel showed the same amide I peaks at ~1660 cm^{-1}, demonstrating amide bond in protein capsid of M13 phage (**Figure 3.5c**). In addition, the hydrogel exhibited amide II (~1570 cm^{-1}), which is also seen for BSA suspension, and amide III bonds (~1280 cm^{-1}). There are multiple new absorption peaks (aside from those shared with glutaraldehyde, BSA solution, and M13 suspension) that suggest new functional groups/new compounds formed. The UV-vis spectrum further showed that the hybrid M13-BSA hydrogel at 50 nm, whereas the phage suspension and BSA solution had a sharp absorption peaks at λ=280 nm, a typical absorption peak for proteins (**Figure 3.5d**).
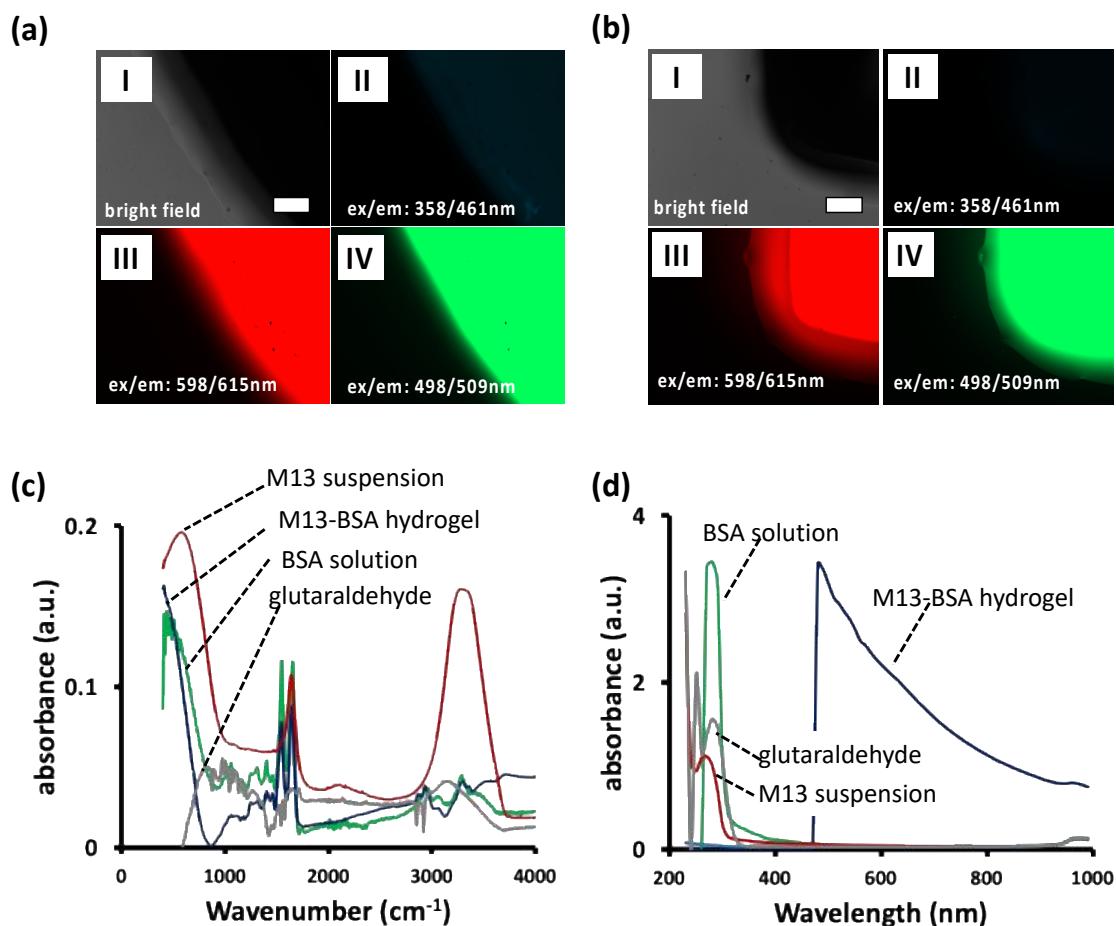
Figure 3.5- *(**a**) Fluorescence micrographs for hydrogel made with 3% BSA: I. brightfield, II. hydrogel excited at 358 nm and imaged using a λ = 461 nm optical filter, III. hydrogel excited at 498 nm and imaged using a λ = 509 nm optical filter, IV. hydrogel excited at 598 nm and imaged using a λ = 615 nm optical filter. Scale bar= 200 μm. (**b**) Fluorescence micrographs for hydrogel made with 1% BSA and 2×10^{12} PFU/mL M13, using the same filters as part c. The gain was kept constant for all three excitation/emission pairs. Scale bar= 200 μm. (**c**) FTIR spectra for M13-BSA hydrogel, BSA hydrogel, and BSA solution. (**d**) UV-Vis spectra of BSA solution, M13 suspension and BSA-M13 hydrogel showing a distinctive peak for the hydrogel.*

2.3. Self-healing capability and bioactivity of hybrid M13 hydrogels

The hybrid M13-BSA hydrogels prepared with 1% BSA exhibited repetitive self-healing capability at room temperature (**Figure 3.6a**). When the hydrogels, cut with a razor blade were incubated at room temperature in the presence of 2.6 mM CaCl$_2$ (extracellular

physiological levels) the hydrogels started to show signs of healing within hours, completely

fusing back together into an intact hydrogel in 24 hrs. Hybrid BSA-M13 hydrogels with different BSA concentrations (1% and 2%) also fused together in the presences of Ca^{2+} (**Figure 3.6b**). Interestingly, the fused hydrogel showed a comparable lower compression modulus to the intact hydrogels (~0.5 vs ~0.8 KPa for the intact hybrid hydrogels with 2% BSA) (**Figure 3.6c**), suggesting an almost biomimetic degree of self-healing with minimum
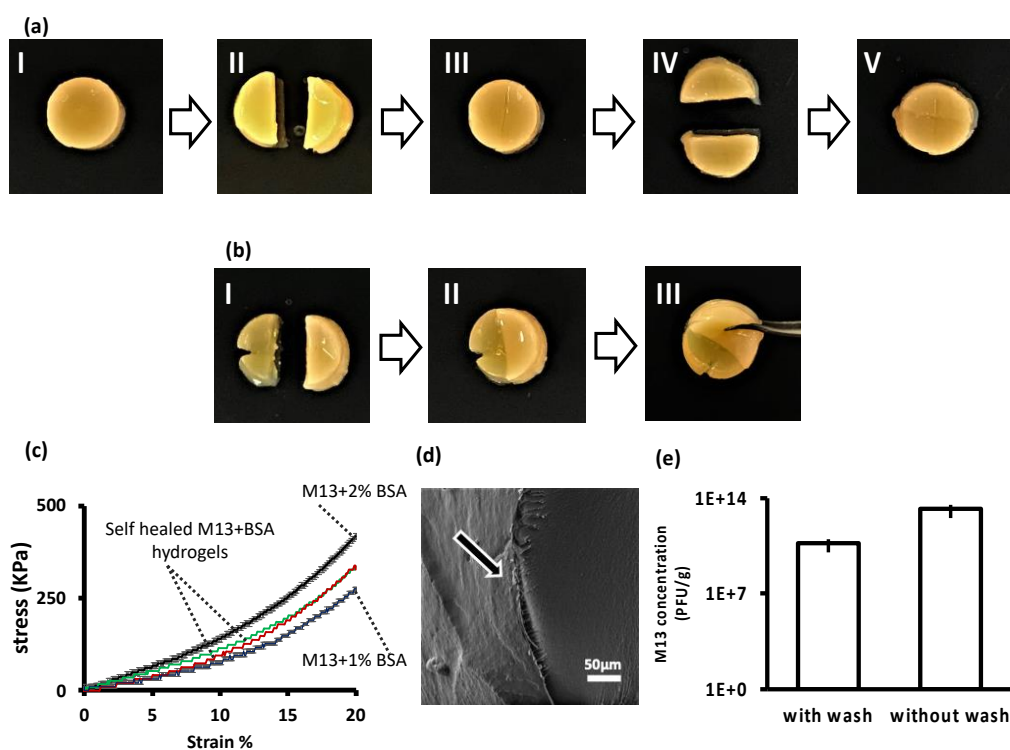
*Figure 3.6- (**a**) Phage hydrogel (2×10^{12} PFU/mL of phage+ 1% BSA) before and after repetitive healing in a 2.4 mM CaCl₂. I. hydrogel made cut with a scalpel, II. Self-healed hydrogel after 24 hrs of incubation, III, IV. Same self-healed hydrogel, cut at a different location, marked by broken line, V. hydrogel, self-healed after the second cut. Both scars are visible in the image. (**b**) Self-healing of two different hybrid hydrogels made with different BSA concentrations. I. Two different hydrogels, one nicked for clarity II. The self-healed gel after incubation in 2.4 mM CaCl₂, III. Demonstrating the stability of the healed region to withstand the weight of the gel. (**c**) compression behavior for M13 hydrogel before and after self-healing in different BSA concentrations. (**d**) SEM images of M13 hydrogel surface after self-healing, arrow shows the location of the scar. (**e**) Bioactive property of M13 hydrogels demonstrated by the ability of M13 in the hydrogel to infect bacterial cells. The wash waters from the gels did not exhibit detectable levels of free M13.*

compromise in mechanical properties. Electron microscopy of the fused gel showed a scar than ran across the body of the gel, showing the layers were fused together at the microscale (**Figure 3.6d**). It has been reported that BSA is physically crosslinked in the presence of Ca^{2+},[19] which may explain the self-healing property of our hybrid M13-BSA hydrogels. However, for BSA to be physically crosslinked with Ca^{2+}, the protein must be first heated to thermally unfold the native BSA protein and form fibrillar BSA aggregates, then gelation is induced by adding fresh native BSA into the solution in the presence of Ca^{2+} at room temperature.[19] There are no reports of BSA being physically crosslinked with Ca^{2+} at room temperature without an initial step of heat-induced aggregation. The observation that our hybrid M13-BSA hydrogels heal under physiological conditions suggests that these hydrogels can be expected to exhibit self-healing similar to biological tissue where the healing processes are autonomously triggered after the damage.

We further confirmed the biological activity of the hybrid M13-BSA phage hydrogels by probing the ability of the M13 phage crosslinked inside the hydrogel to infect their bacterial host. We incubated the hydrogels with *E. coli* ER2738 (5hrs, 37℃), the culture showed a relatively high titer of phage suggesting the M13 phage inside the hydrogel, even though fixed in a matrix and chemically crosslinked, was still biologically active and able to infect its host bacteria and propagate itself (**Figure 3.6e**). To rule out the possibility of M13 leaking out of the hydrogels, we compared the results for freshly prepared hydrogels with hydrogels that were washed in Millipore water (10 water changes, 25 mL each). The washed hydrogel resulted in the same level of propagated phage as the non-washed hydrogel, when incubated with host bacteria (**Figure 3.6e**). This result also indicates that the any possible residues of the glutaraldehyde crosslinker used to prepare the hydrogel, was below toxicity levels to bacteria, because the bacteria were physiologically active to propagate the phage. We further checked the phage count in the wash waters used to wash the hybrid hydrogels. The concentration of M13 phage in the wash waters was below detection limit of the standard plaque assay, indicating minimal leaking out of M13 phage out of the hydrogels. This evidence further confirms that m13 propagation in the presence of hydrogels in not a result of leaking of free M13 phage, but mainly a result of the

preserved biological activity of M13 in our hydrogels. These observations suggest that the M13 phage inside he hybrid hydrogels are very much biologically active and not deactivated in the presence of glutaraldehyde or because of being physically bound to a matrix. The process of phage infection of a bacterial cell is complex and comprised of multiple steps. A 50 KDa protein on tip of the phage fiber has to bind to the bacterial cell to initiate the insertion of the M13 genome into the bacterial cell and start the infection and M13 propagation cycle.[7] This means that as long as the binding proteins are active, even if M13 filaments are not available to freely diffuse through the environment and bind to their host cells they can still infect host bacteria, thus maintaining their cherished biological activity in the hydrogel. M13 bioactivity in the hydrogel matrix offers possibilities for the preparation of bioactive hydrogels that offer multiple different types of biorecognition (engineered through recombinant DNA techniques and/or phage display).

3. Conclusion

We report the synergistic action of M13 filamentous phage and BSA, a small globular protein leading to the formation of a hybrid hydrogel. Neither the M13 phage, nor BSA can from hydrogels at the concentrations used in this work when reacted with 1% glutaraldehyde. We believe that this synergy is a result of a shift in the phase diagram of the M13 phage suspension, causing an early onset of formation of liquid crystalline ordered domains. We showed in a previous publication that the formation of these self-organized domains at very high M13 concentrations was responsible for the formation M13 hydrogels. In the current report, however, we managed to form M13hydrogels at concentrations 100× lower than the onset of formation of smectic phase, in the presence of BSA protein. The Presence of M13 phage in the hybrid hydrogels significantly increased the swelling ratio of the M13-BSA hydrogels (>2×) over BSA only hydrogels, which we hypothesize is because of the marked change in pore structure between hybrid BSA-M13 hydrogels and BSA only hydrogels, as observed in electron micrographs. Presence of BSA, however, worked to increase (>5×) the compression Modulus of the hybrid M13-BSA hydrogels over M13 hydrogels with minute amounts of BSA. This indicate a compromise between ability to pack water and mechanical strength of the hydrogel, which must be

accounted for when designing hybrid M13-BSA hydrogels based on the final application. Our hybrid hydrogels exhibit characteristics that make them attractive for biomedical applications, namely autofluorescence in three wavelengths, self-healing under physiological conditions with minimal loss of mechanical strength and preserved biological activity, towards their host bacterial cells. Our report highlights the utility of hybrid M13 hydrogels for preparation of bioactive multifunctional material as well as the importance of further mechanistic investigations into the nature of the phase diagram for filamentous phage in the presence of different proteins of biological relevance, which might open avenues for the development of stimulus-responsive biomaterials with M13 phage.

4. Supplementary Information
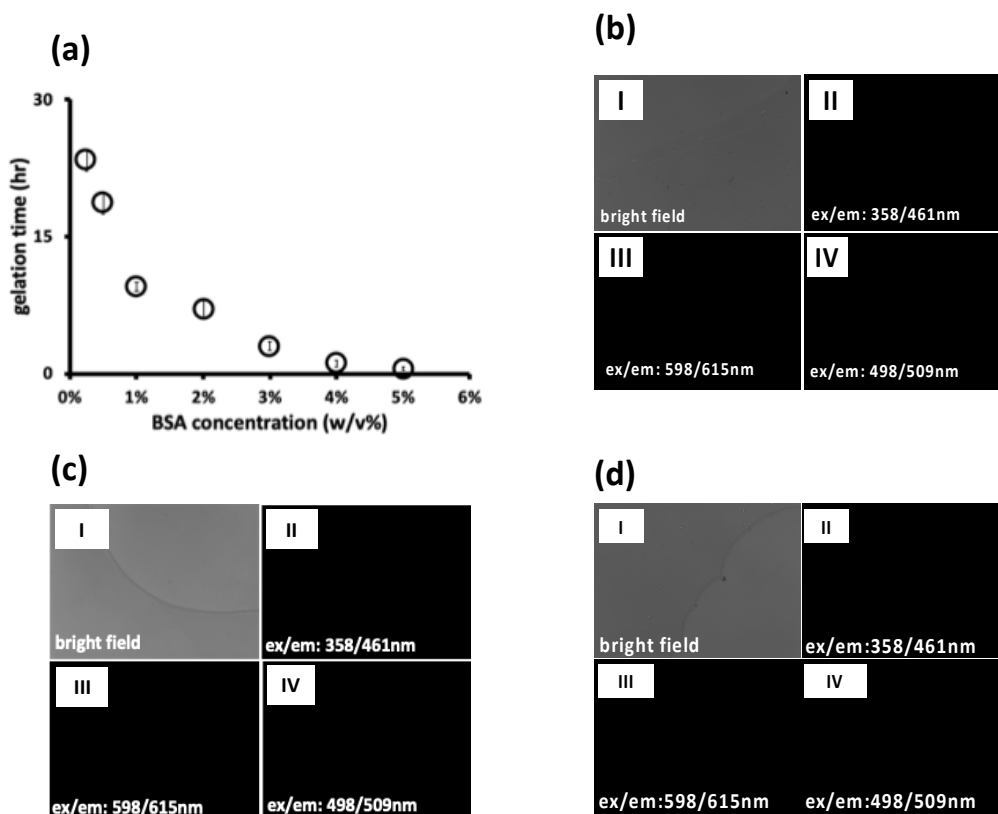
Figure S3.7- *(**a**) Gelation time for hybrid M13-BSA hydrogels. Brightfield and fluorescence micrographs of (**b**) BSA solution; (**c**) 3×10^{12} PFU/mL M13 phage; (**d**) glutaraldehyde.*

5. References

1   Mohammed, N., Grishkewich, N., Berry, R. M. & Tam, K. C. Cellulose nanocrystal–alginate hydrogel beads as novel adsorbents for organic dyes in aqueous solutions. *Cellulose*, (2015).

2   Xu, X. *et al.* Preparation and in vitro characterization of thermosensitive and mucoadhesive hydrogels for nasal delivery of phenylephrine hydrochloride. *Eur. J. Pharm. Biopharm.* **88**, 998-1004, (2014).

3   Olde Damink, L. H. H. *et al.* Glutaraldehyde as a crosslinking agent for collagen-based biomaterials. *J. Mater. Sci. Mater. Med.* **6**, 460-472, (1995).

4   Kim, U.-J. *et al.* Structure and Properties of Silk Hydrogels. *Biomacromolecules* **5**, 786-792, (2004).

5   Nieto-Suárez, M., López-Quintela, M. A. & Lazzari, M. Preparation and characterization of crosslinked chitosan/gelatin scaffolds by ice segregation induced self-assembly. *Carbohydr. Polym.* **141**, 175-183, (2016).

6   Krall, N., da Cruz, F. P., Boutureira, O. & Bernardes, G. J. L. Site-selective protein-modification chemistry for basic biology and drug development. *Nat. Chem.* **8**, 103, (2015).

7   Calendar, R. L. *The Bacteriophages*. second edn, (Oxford University Press, 2006).

8   Rakonjac, J. *Filamentous Bacteriophages: Biology and Applications*. (2012).

9   Lee, J. H. *et al.* Production of tunable nanomaterials using hierarchically assembled bacteriophages. *Nat. Protocols* **12**, 1999-2013, (2017).

10   Dogic, Z. & Fraden, S. Ordered phases of filamentous viruses. *Current Opinion in Colloid & Interface Science* **11**, 47-55, (2006).

11   Lee, S.-W., Mao, C., Flynn, C. E. & Belcher, A. M. Ordering of Quantum Dots Using Genetically Engineered Viruses. *Science* **296**, 892-895, (2002).

12   Lee, S. W., Lee, S. K. & Belcher, A. M. Virus-Based Alignment of Inorganic, Organic, and Biological Nanosized Materials. *Adv. Mater.* **15**, 689-692, (2003).

13   Lee, J. H. *et al.* Phage-Based Structural Color Sensors and Their Pattern Recognition Sensing System. *ACS Nano* **11**, 3632-3641, (2017).

14   Sawada, T. *et al.* Filamentous Virus-based Assembly: Their Oriented Structures and Thermal Diffusivity. *Sci. Rep.* **8**, 5412, (2018).

15   Adams, M., Dogic, Z., Keller, S. L. & Fraden, S. Entropically driven microphase transitions in mixtures of colloidal rods and spheres. *Nature* **393**, 349, (1998).

16   Sambrook, J. & Russell, D. W. *Molecular cloning: a laboratory manual*. 3 edn, (Cold Spring Harbour laboratory Press, 2001).

17   Kropinski, A. M., Mazzocco, A., Waddell, T. E., Lingohr, E. & Johnson, R. P. in *Bacteriophages: Methods and Protocols, Volume 1: Isolation, Characterization, and Interactions*   (eds Martha R. J. Clokie & Andrew M. Kropinski) 69-76 (Humana Press, 2009).

18   Chung, W.-J., Lee, D.-Y. & Yoo, S. Y. Chemical modulation of M13 bacteriophage and its functional opportunities for nanomedicine. *International Journal of Nanomedicine* **9**, 5825-5836, (2014).

19   Chen, J., Dong, Q., Ma, X., Fan, T.-H. & Lei, Y. Repetitive Biomimetic Self-healing of Ca^{2+}-Induced Nanocomposite Protein Hydrogels. *Sci. Rep.* **6**, 30804, (2016).

Chapter 4 – Future perspective

1. Challenges

Most phage hydrogels (containing only filamentous phage and a crosslinker and no extra gelling agents) have been prepared with very high phage concentrations. Obtaining such high phage concentrations ($>10^{14}\ PFU/mL$) was the main challenge in preparing pure phage hydrogels. These preparations must be pure and free of bacterial cell debris, lipopolysaccharides (which can be toxic), and bacterial proteins which could interfere with the chemistry and lead to non-reproducible outcome and also affect biocompatibility. In my experience, producing a high concentration ($5 \times 10^{14}\ PFU/mL$) was a highly laborious task that required a week on average for producing 500 μL of M13 suspension.

Another challenge for crosslinking viral nanoparticles, in general, is ensuring that the crosslinking chemistry does not denature the phage coat proteins. Aside from being new and interesting materials assembled from nano-building block from bottom up, phage hydrogels are meant to serve a void in the hydrogel arena, namely bioactive hydrogels that are capable of specific interaction with a wide array of organic and inorganic targets. Therefore, care must be taken to preserve the bioactivity of the phage surface proteins.

2. Impact and Future Directions

The main impact of this investigation is to present M13 phage as a powerful tool for making advanced, multifunctional material, without the need to supplement with responsive crosslinkers or synthetic nanoparticles. We demonstrated the unique properties of M13 hydrogels that will pave the road for development of multifunctional bioactive hydrogels for applications in biomedical engineering or environmental engineering, in the future.

Our three main proposals for the future directions of this work is to 1- investigate the mechanism behind self-healing and autofluorescence for M13 phage hydrogels, 2- the effect of various environmental conditions on self-healing, specifically whether other small globular proteins can cause the same effect as BSA, and 3- preparation of bioactive hydrogels with genetically engineered filamentous phage for applications in biomedical engineering.